

Electronic Supplementary Information (ESI)

Dissecting the chloride-nitrate anion transport assay

Yufeng Yang,^{a,b} Xin Wu,^c Nathalie Busschaert,^a Hiroyuki Furuta^b and Philip A. Gale^{*c}

^a *Chemistry, University of Southampton, Southampton, SO17 1BJ, UK*

^b *Department of Chemistry and Biochemistry, Kyushu University, Fukuoka, 819-0395, Japan*

^c *School of Chemistry, The University of Sydney, NSW 2006, Australia*

*Corresponding author. Email: philip.gale@sydney.edu.au

Contents

1. General.....	S2
2. Synthesis of compound 4	S3
3. UV-vis binding studies	S6
4. ISE chloride-nitrate exchange assay	S13
4.1 General.....	S13
4.2 Kinetic data	S14
5. HPTS assay	S15
5.1 General.....	S15
5.2 Hill plots for Cl ⁻ transport	S16
5.3 Hill plots for NO ₃ ⁻ transport.....	S19
6. Osmotic assay	S22
6.1 General.....	S22
6.2 Hill plots for Cl ⁻ transport	S23
6.3 Hill plots for NO ₃ ⁻ transport.....	S25
6.4 Br ⁻ transport.....	S27
6.5 Single concentration comparison of anion transport.....	S28
7. Correlation between binding selectivity and transport selectivity	S29
8. Normalised anion transport activities	S30
9. Computational studies.....	S30
10. References.....	S31

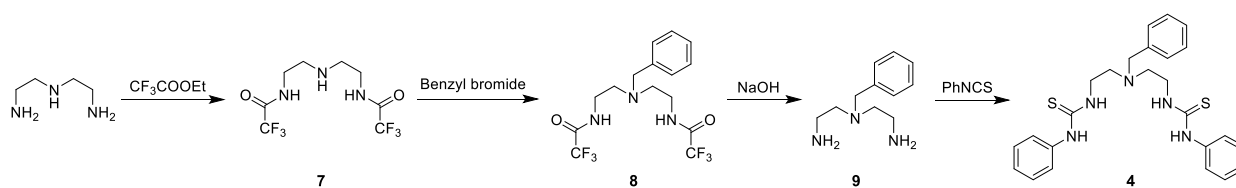
1. General

POPC was purchased from Avanti Polar Lipids. Other commercially available chemicals were purchased from Sigma-Aldrich, Alfa-Aesar, or Fisher Scientific, and used as received. NMR spectra were recorded on a Bruker AV300 spectrometer. High resolution mass spectrometry (HRMS) was performed on a Bruker Apex III. Infrared (IR) spectra were recorded on a Matterson Satellite (ATR). UV-vis absorption spectra were obtained on an Agilent Cary-100 UV-vis Spectrophotometer equipped with a stirrer plate and a temperature controller. Fluorescence and light scattering measurements were performed using an Agilent Cary Eclipse Fluorescence Spectrophotometer equipped with a stirrer plate and a temperature controller. Compounds **1**¹, **2**¹, **3**¹, **5**² and **6**³ were synthesized following reported procedures.

Abbreviations

DMSO	Dimethyl sulfoxide
ESI	Electrospray ionisation
HEPES	4-(2-Hydroxyethyl)-1-piperazineethanesulfonic acid
HPTS	8-Hydroxypyrene-1,3,6-trisulfonic acid
HRMS	High resolution mass spectrometry
IR	Infrared
ISE	Ion-selective electrode
LUV	Large unilamellar vesicles
NMDG	<i>N</i> -methyl-D-glucamine
NMR	Nuclear magnetic resonance
POPC	1-Palmitoyl-2-oleoyl- <i>sn</i> -glycero-3-phosphocholine
TBA	Tetrabutylammonium
UV-vis	Ultraviolet-visible
Vln	Valinomycin

2. Synthesis of compound 4



Scheme S1 Synthesis of compound 4

***N,N'*-(azanediylbis(ethane-2,1-diyl))bis(2,2,2-trifluoroacetamide) (7).** A mixture of 2.68 mL diethylenetriamine (25 mmol) and 10.1 mL ethyltrifluoro acetate (85 mmol, 3.5 eq) in 50 mL acetonitrile containing 0.5 mL water was refluxed for 18 h. The solvents were removed under reduced pressure and the residue was recrystallised from 1:1 acetonitrile-Et₂O. The precipitate was filtered off and washed with cold Et₂O to give a white solid (7.35 g, 24.8 mmol). Yield: 99%; ¹H NMR (300 MHz, DMSO-*d*₆) δ ppm 3.14 (t, $J = 6.22$ Hz, 4 H), 3.50 (q, $J = 5.85$ Hz, 4 H), 8.70 (br. s., 1 H), 9.59 (br. s., 2 H); ¹³C NMR (75 MHz, DMSO-*d*₆) δ ppm 35.70, 45.17, 115.65 (q, $J = 288.60$ Hz), 156.60 (q, $J = 35.38$ Hz), 158.96.

***N,N'*-(benzylazanediyl)bis(ethane-2,1-diyl)bis(2,2,2-trifluoroacetamide) (8).** A mixture of 4.00 g compound 7 (13.5 mmol) and 4.00 mL triethylamine (28.7 mmol) in acetonitrile (50 mL) was stirred for 2 h at 50°C under nitrogen. 2.50 mL benzyl bromide (21.0 mmol) was added and the solution was stirred for 48 h at 50°C under nitrogen. Acetonitrile was removed under reduced pressure and the residue was purified by column chromatography (5% methanol in dichloromethane), followed by recrystallisation from 1:1 dichloromethane-hexane. The resulting precipitate was filtered off and washed with hexane to give a white solid (2.72 g, 7.04 mmol). Yield: 53%; ¹H NMR (300 MHz, DMSO-*d*₆) δ ppm 2.59 (t, $J = 6.59$ Hz, 4 H), 3.29 (q, $J = 6.03$ Hz, 4 H), 3.60 (s, 2 H), 7.25 (m, 5 H), 9.21 (br. s., 2 H); ¹³C NMR (75 MHz, DMSO-*d*₆) δ ppm 37.06, 51.53, 57.49, 115.90 (q, $J = 289.70$ Hz), 126.83, 128.04, 128.38, 139.06, 156.19 (q, $J = 35.38$ Hz); HRMS (ESI) for C₁₅H₁₈F₆N₃O₂ [M+H]⁺: $m/z = 386.1298$ (calcd), 386.1304 (found).

***N*¹-(2-aminoethyl)-*N*¹-benzylethane-1,2-diamine (9).** Compound 8 (2.50 g, 6.4 mmol) was dissolved in 25 mL methanol. A solution of 2.50 g NaOH in 25 mL water was added and the mixture was stirred overnight at room temperature. Methanol was removed under reduced pressure and the remaining aqueous phase was extracted with DCM (3 × 50 mL). The combined organic phases were dried with MgSO₄ and the MgSO₄ was subsequently removed by filtration. DCM was removed under reduced pressure and dried overnight *in vacuo* to give a clear oil (0.94 g, 4.83 mmol). Compound 9 was used without further purification. Yield: 75%; ¹H NMR (300 MHz, CDCl₃) δ ppm 2.52 (br. s., 4 H), 2.76 (br. s., 4 H), 3.56 (br. s., 2 H), 7.20 (m, 5 H); ¹³C NMR (75 MHz, CDCl₃) δ ppm 38.92, 55.55, 58.17, 127.09, 128.29, 129.10, 138.45.

1,1'-((benzylazanediy)bis(ethane-2,1-diyl))bis(3-phenylthiourea) (4). A mixture of 0.30 g compound **9** (1.55 mmol), 0.50 g Na₂SO₄ and 2 equivalents of phenyl isothiocyanate in 50 mL DCM was stirred overnight at room temperature under nitrogen. 20 mL water was added to remove Na₂SO₄. The DCM layer was removed and the aqueous phase was further extracted with DCM (2x50 mL). The combined organic layers were dried with MgSO₄ and the MgSO₄ was subsequently removed by filtration. DCM was removed under reduced pressure and the crude oil was recrystallised from 1:1 DCM-hexane. The precipitate was filtered off and washed with hexane. The white solid was then dried overnight *in vacuo* (0.66 g, 1.42 mmol). Yield: 92%; Mp: 156.0-156.4°C; ¹H NMR (300 MHz, DMSO-*d*₆) δ ppm 2.64 (t, *J*=6.59 Hz, 4 H), 3.60 (q, *J*=5.65 Hz, 4 H), 3.64 (s, 2 H), 7.14 (m, 2 H), 7.22 (m, 5 H), 7.35 (m, 8 H), 7.55 (br. s., 3 H), 9.62 (br. s., 3 H); ¹³C NMR (75 MHz, DMSO-*d*₆) δ ppm 41.60, 51.55, 57.61, 123.41, 124.42, 126.75, 128.09, 128.52, 128.77, 138.96, 138.96, 180.00; IR (film): ν = 3160 (*br*, NH stretch), 1520 (CS stretch) cm⁻¹; HRMS (ESI) for C₂₅H₃₀N₅S₂ [M+H]⁺: *m/z* = 464.1937 (calcd), 464.1939 (found).

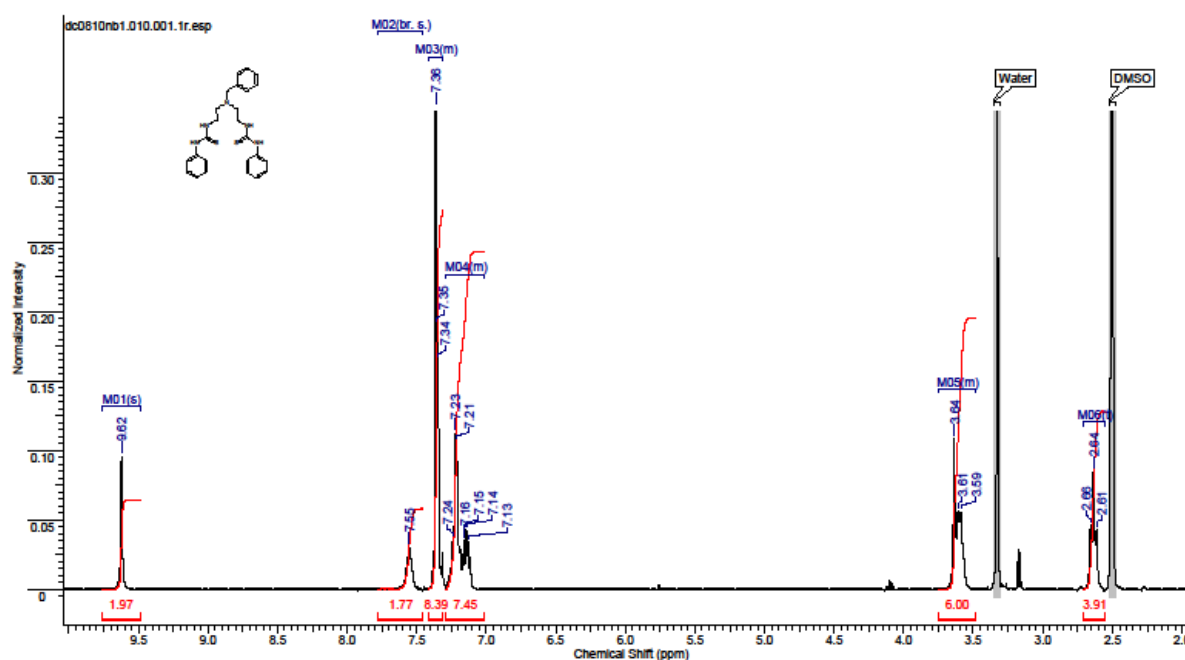


Fig. S1 ¹H NMR (300 MHz) spectrum of **4** in DMSO-*d*₆.

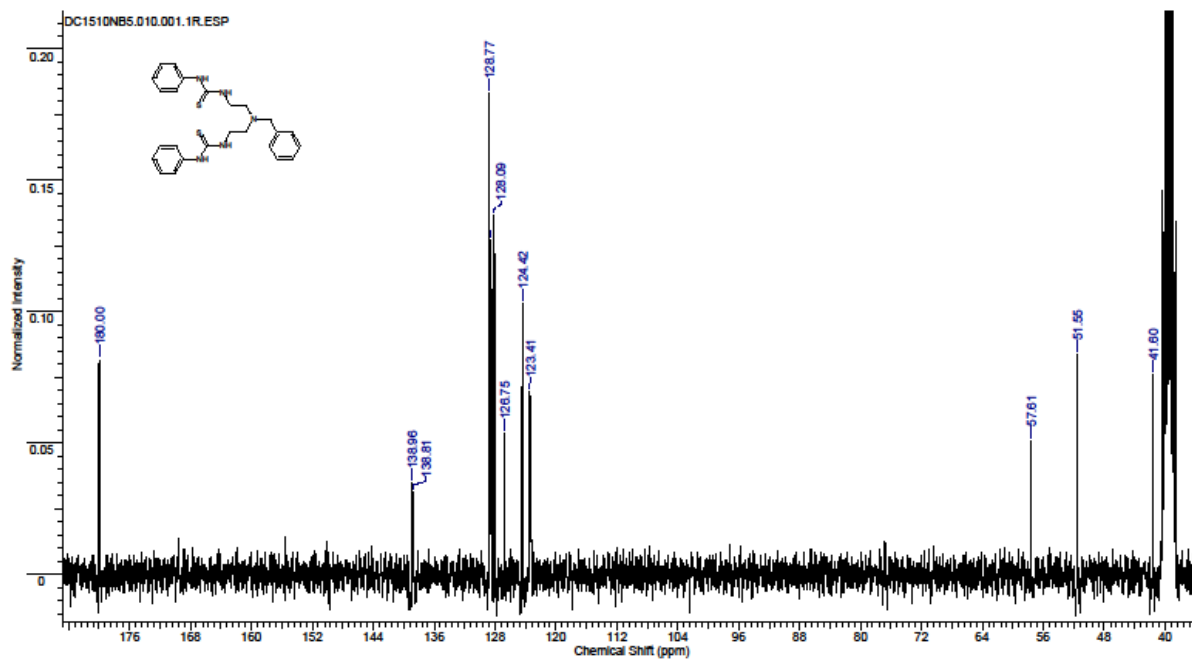


Fig. S2 ^{13}C NMR (75 MHz) spectrum of **4** in $\text{DMSO-}d_6$.

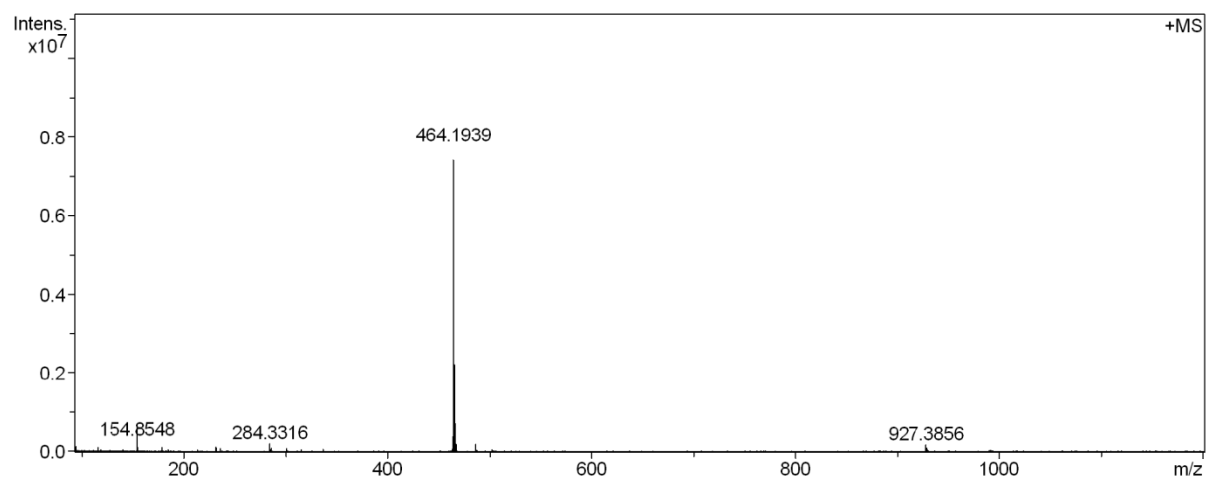


Fig. S3 HRMS (ESI+) of **4**.

3. UV-vis binding studies

UV-vis binding studies were performed by adding an acetonitrile solution containing both the host and the guest (TBACl, TBABr or TBANO₃) into an acetonitrile solution of the host in a quartz cuvette thermostated at 298 K. The UV-vis spectra of the host in the absence and presence of increasing concentration of the guest were measured. The absorbance values at chosen wavelengths were plotted against the guest concentration, and fitted to a 1:1 binding model.

Table S1 Br⁻ association constants and selectivities of compounds **1–6** in acetonitrile at 298 K.

Compound	$K_a(\text{Br}^-) / \text{M}^{-1}$	$S_b(\text{Br}^-/\text{NO}_3^-)^a$	$S_b(\text{Cl}^-/\text{Br}^-)^b$
1	3.3×10^4	13	25
2	1.9×10^3	1.8	9.8
3	1.7×10^3	2.8	14
4	1.4×10^3	6.8	21
5	1.7×10^4	62	100
6	2.2×10^4	44	38

^a Br⁻/NO₃⁻ binding selectivity $S_b(\text{Br}^-/\text{NO}_3^-) = K_a(\text{Br}^-) / K_a(\text{NO}_3^-)$. ^b Cl⁻/Br⁻ binding selectivity $S_b(\text{Cl}^-/\text{Br}^-) = K_a(\text{Cl}^-) / K_a(\text{Br}^-)$.

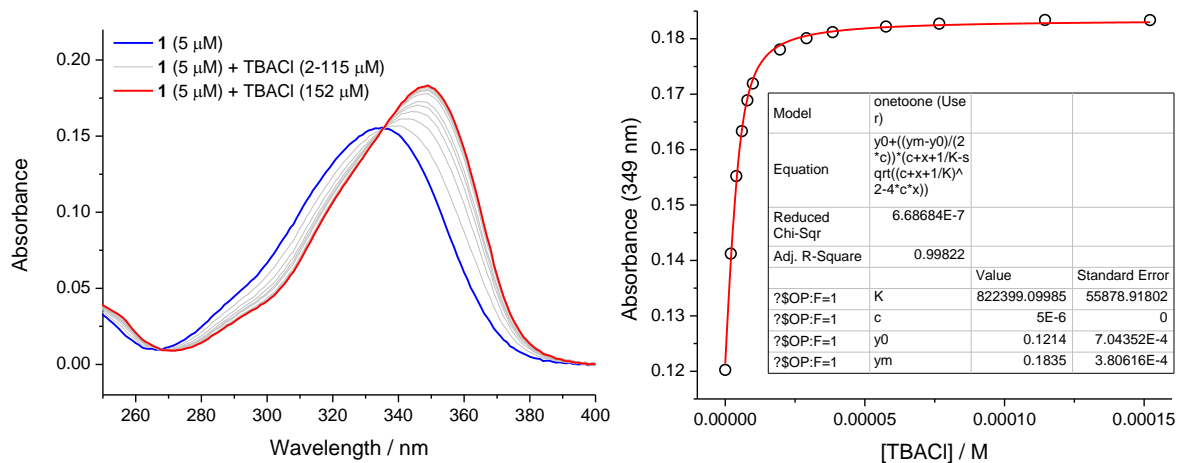


Fig. S4 UV-vis titration of 1 (5 μM) with TBACl (0–152 μM) in CH₃CN at 298 K.

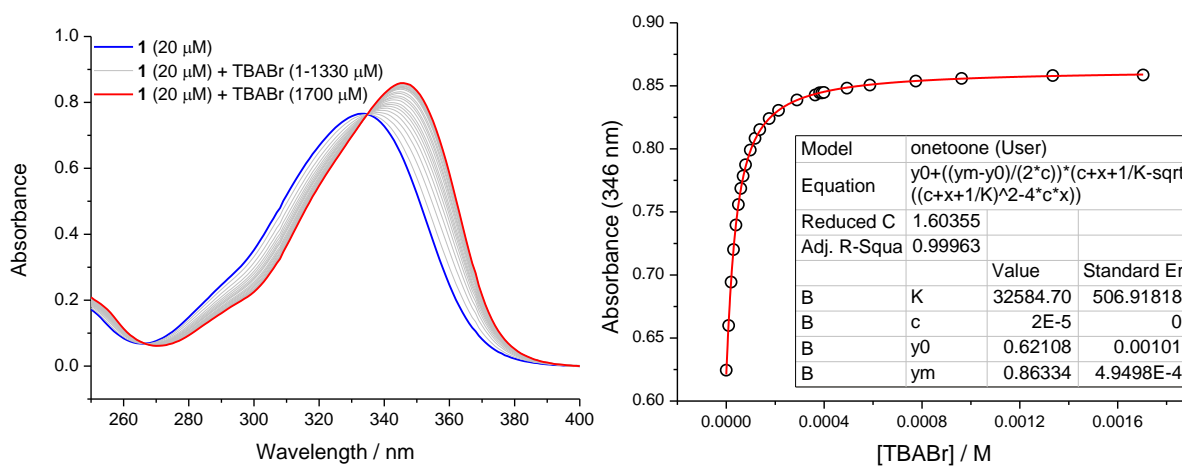


Fig. S5 UV-vis titration of 1 (20 μM) with TBABr (0–1.7 mM) in CH₃CN at 298 K.

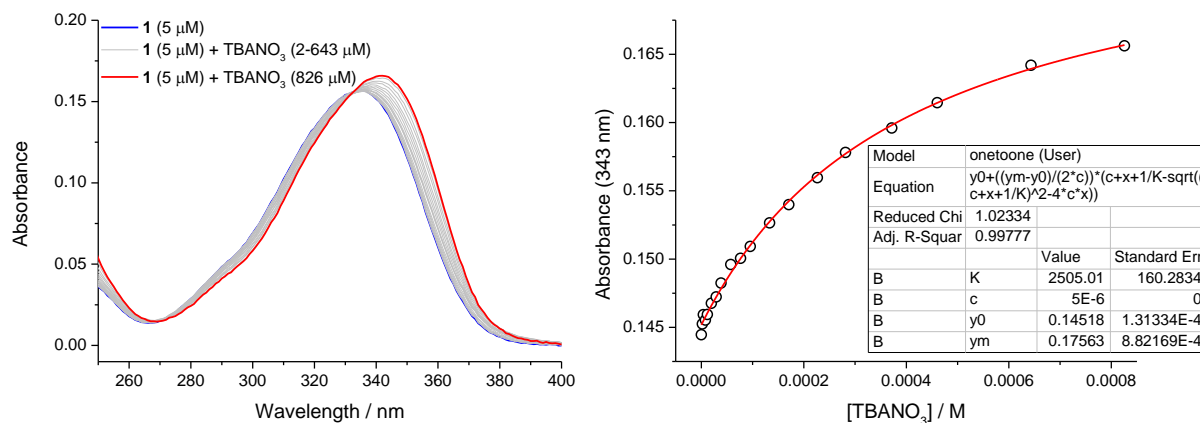


Fig. S6 UV-vis titration of 1 (5 μM) with TBANO₃ (0–826 μM) in CH₃CN at 298 K.

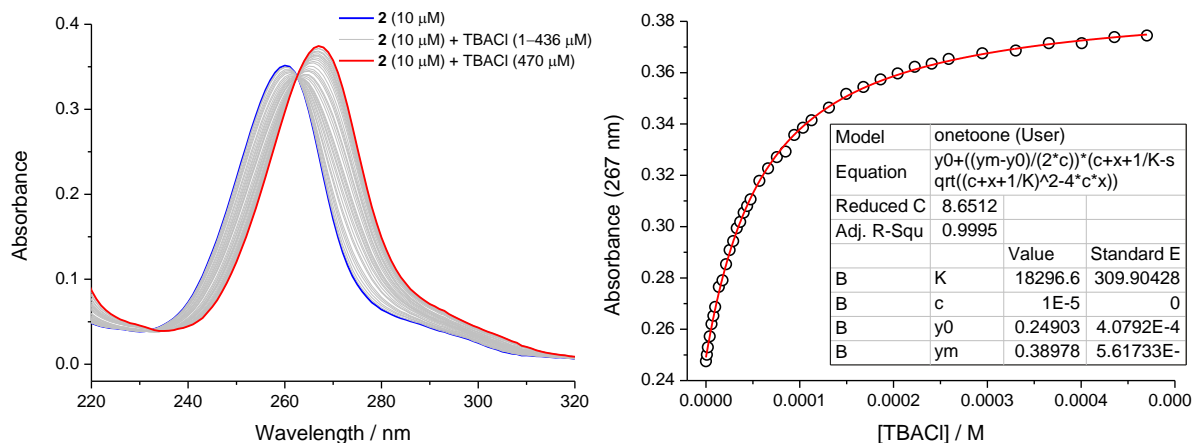


Fig. S7 UV-vis titration of **2** (10 μ M) with TBACl (0–470 μ M) in CH_3CN at 298 K.

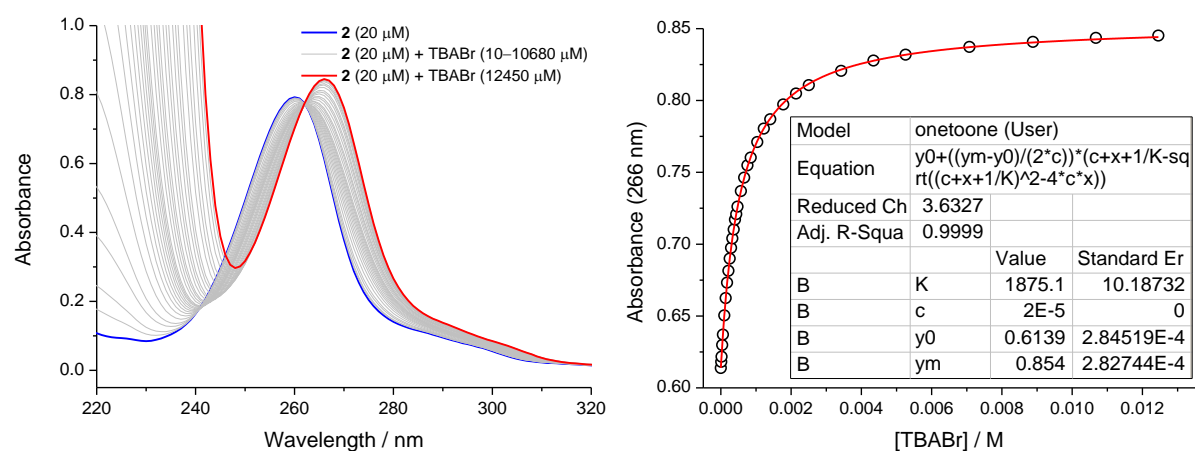


Fig. S8 UV-vis titration of **2** (20 μ M) with TBABr (0–12.4 mM) in CH_3CN at 298 K.

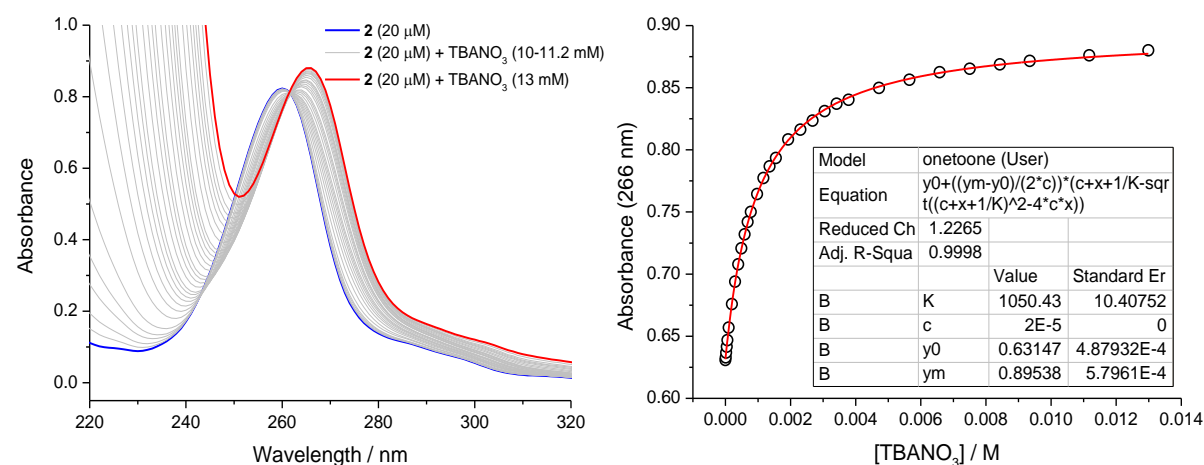


Fig. S9 UV-vis titration of **2** (20 μ M) with TBANO_3 (0–13 mM) in CH_3CN at 298 K.

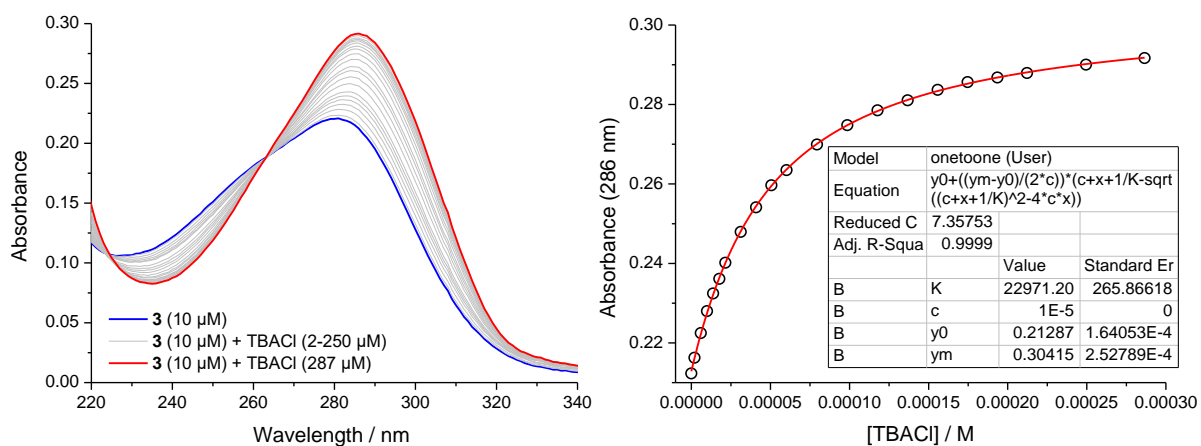


Fig. S10 UV-vis titration of **3** (10 μM) with TBACl (0–287 μM) in CH_3CN at 298 K.

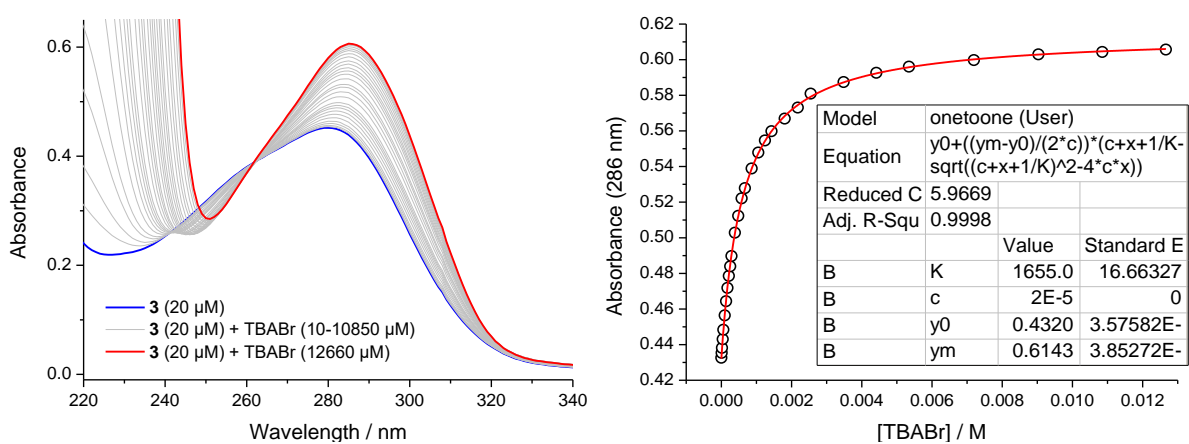


Fig. S11 UV-vis titration of **3** (20 μM) with TBABr (0–12.7 mM) in CH_3CN at 298 K.

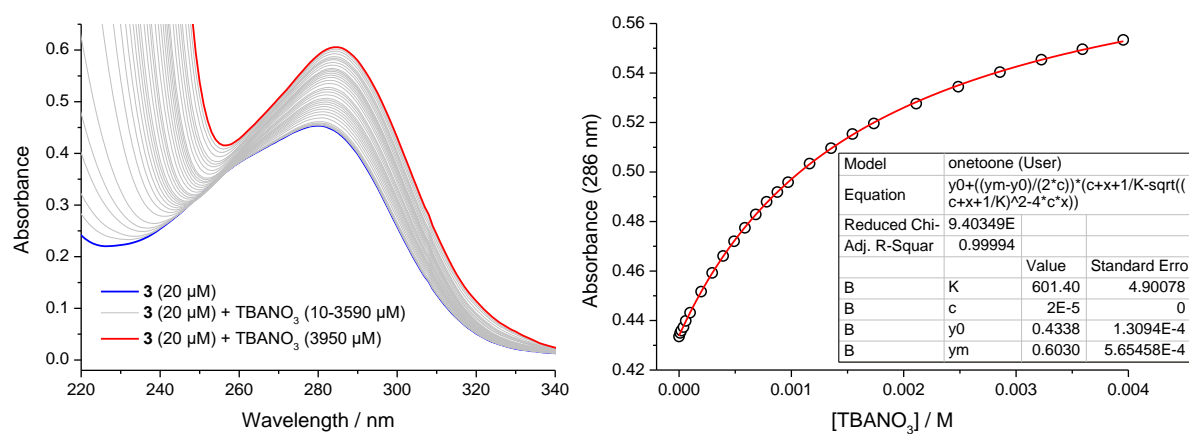


Fig. S12 UV-vis titration of **3** (20 μM) with TBANO_3 (0–3.95 mM) in CH_3CN at 298 K.

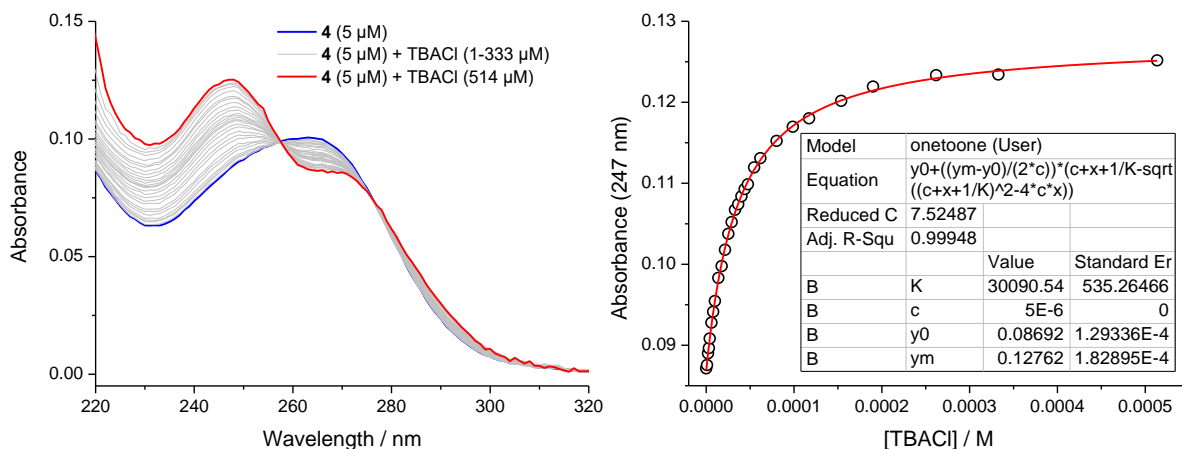


Fig. S13 UV-vis titration of **4** (5 μM) with TBACl (0–514 μM) in CH_3CN at 298 K.

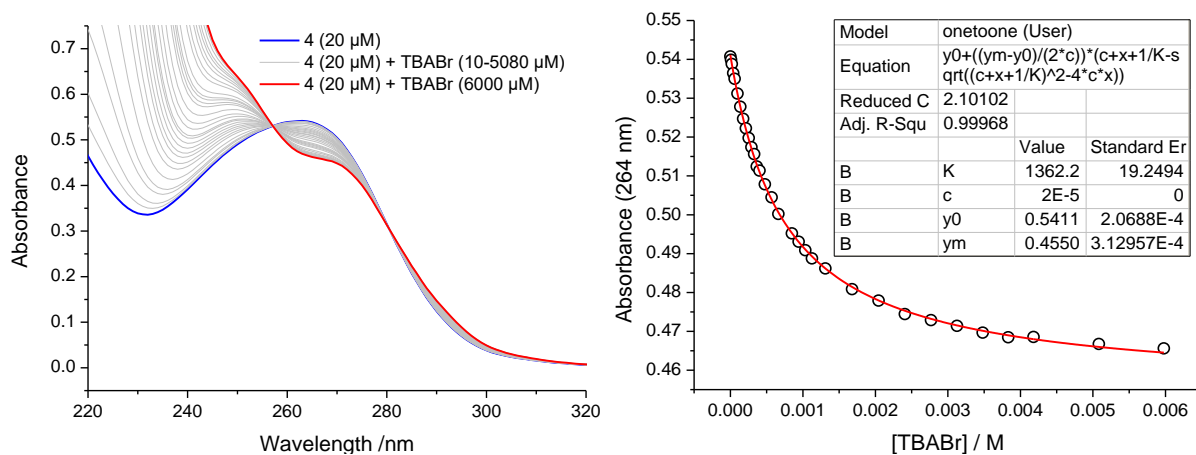


Fig. S14 UV-vis titration of **4** (20 μM) with TBABr (0–6 mM) in CH_3CN at 298 K.

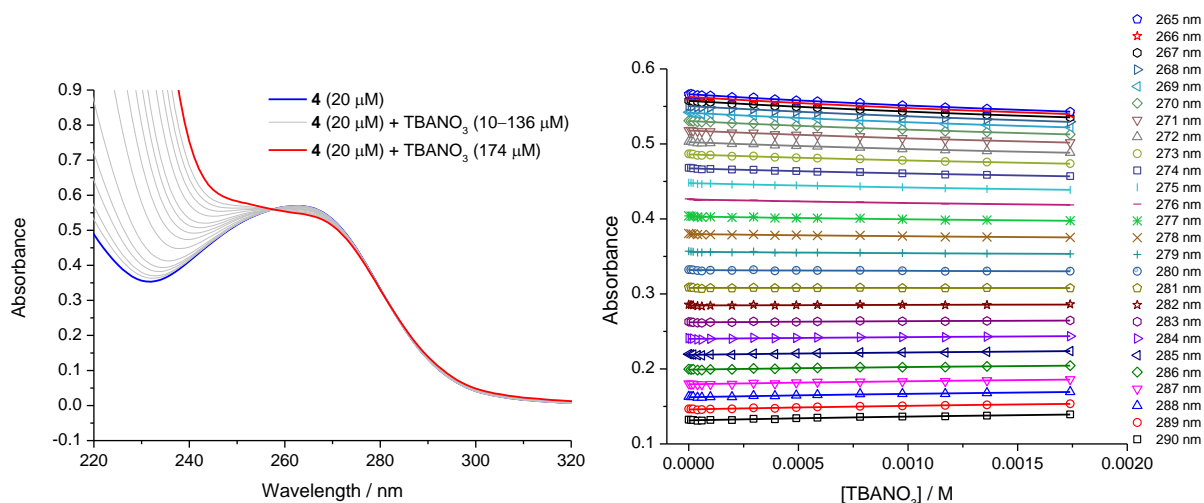


Fig. S15 UV-vis titration of **4** (20 μM) with TBANO_3 (0–174 μM) in CH_3CN at 298 K. Global fitting of 26 absorbance values (265–290 nm) using the online BindFit software⁴ gave an association constant of 210 M^{-1} .

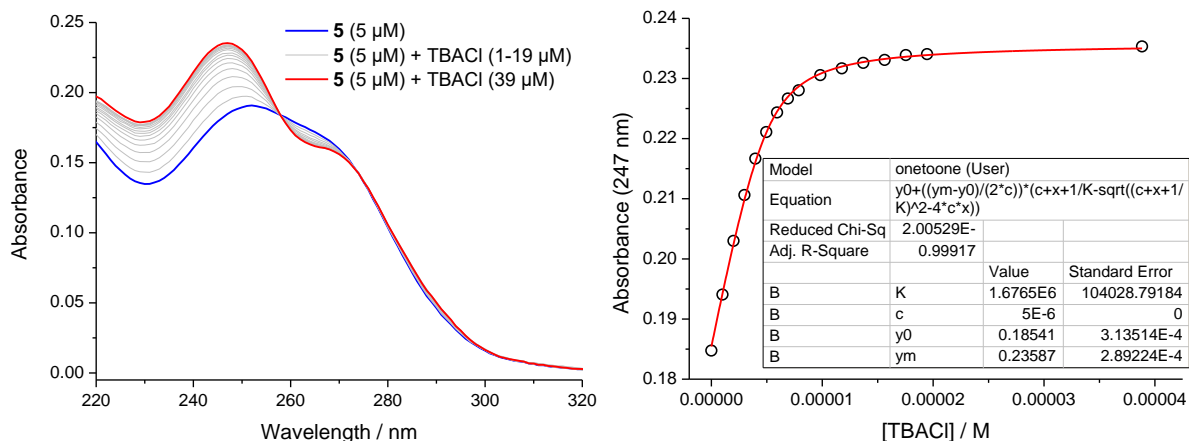


Fig. S16 UV-vis titration of **5** (5 μM) with TBACl (0–39 μM) in CH_3CN at 298 K.

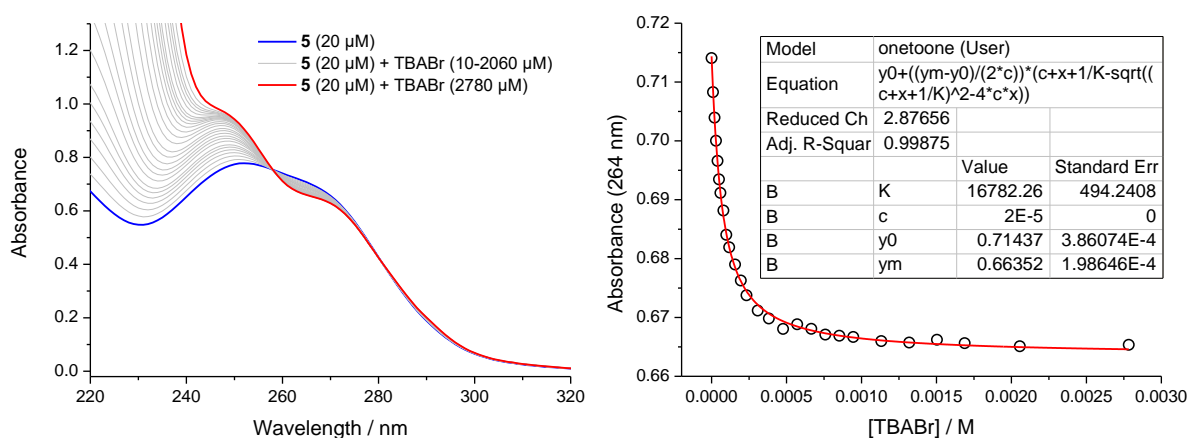


Fig. S17 UV-vis titration of **5** (20 μM) with TBABr (0–2.78 mM) in CH_3CN at 298 K.

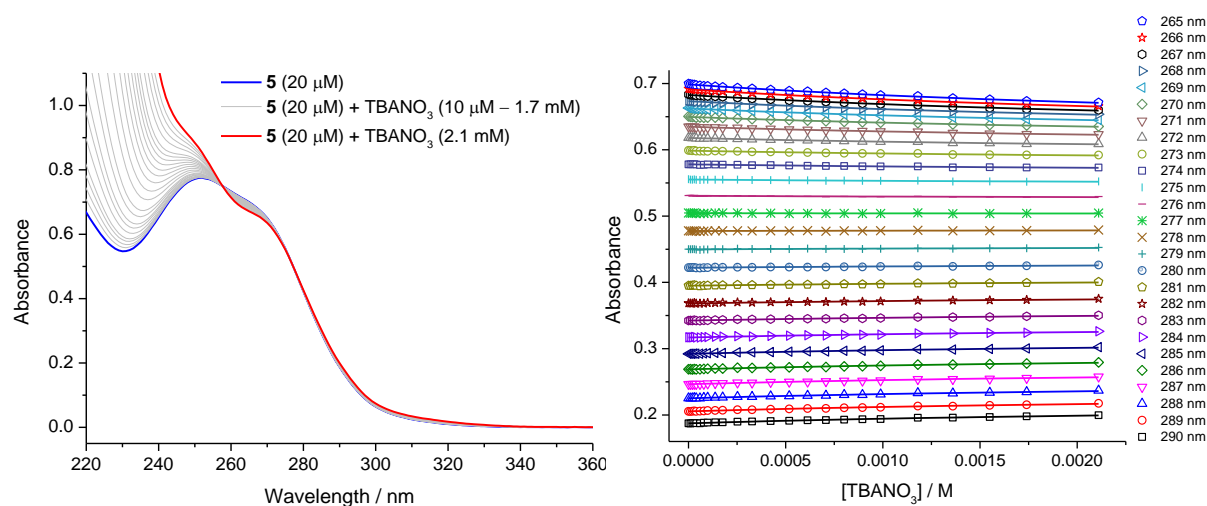


Fig. S18 UV-vis titration of **5** (20 μM) with TBANO_3 (0–2.1 mM) in CH_3CN at 298 K. Global fitting of 26 absorbance values (265–290 nm) using the online BindFit software⁴ gave an association constant of 270 M^{-1} .

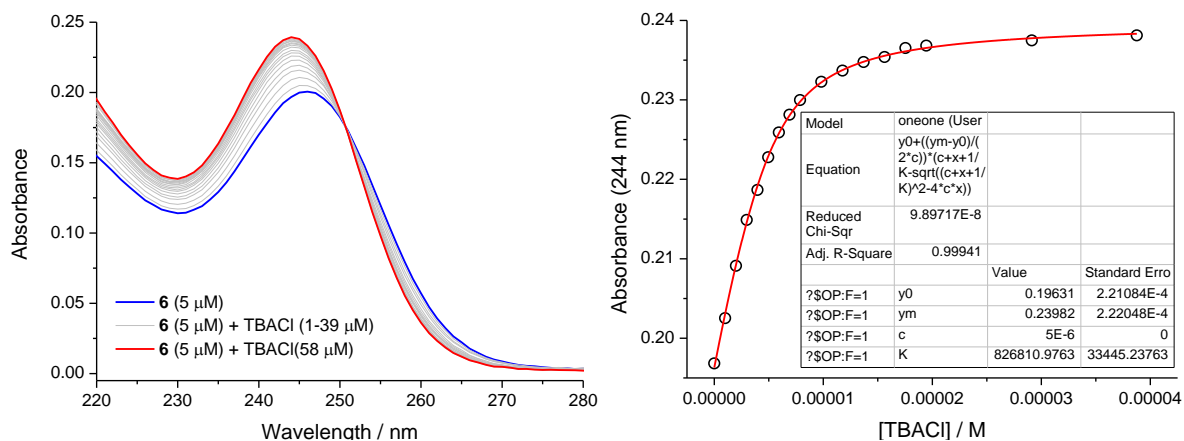


Fig. S19 UV-vis titration of **6** (5 μ M) with TBACl (0–58 μ M) in CH₃CN at 298 K.

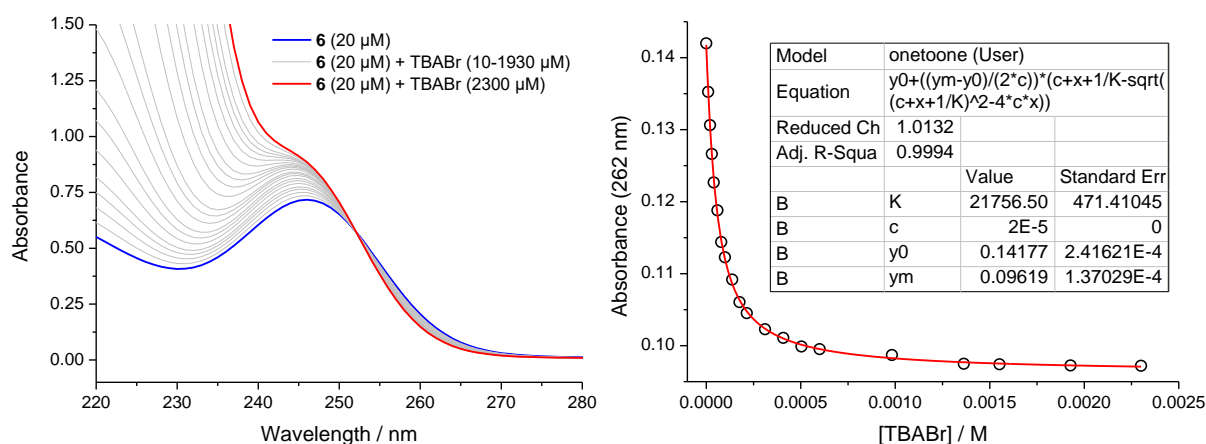


Fig. S20 UV-vis titration of **6** (20 μ M) with TBABr (0–2.3 mM) in CH₃CN at 298 K.

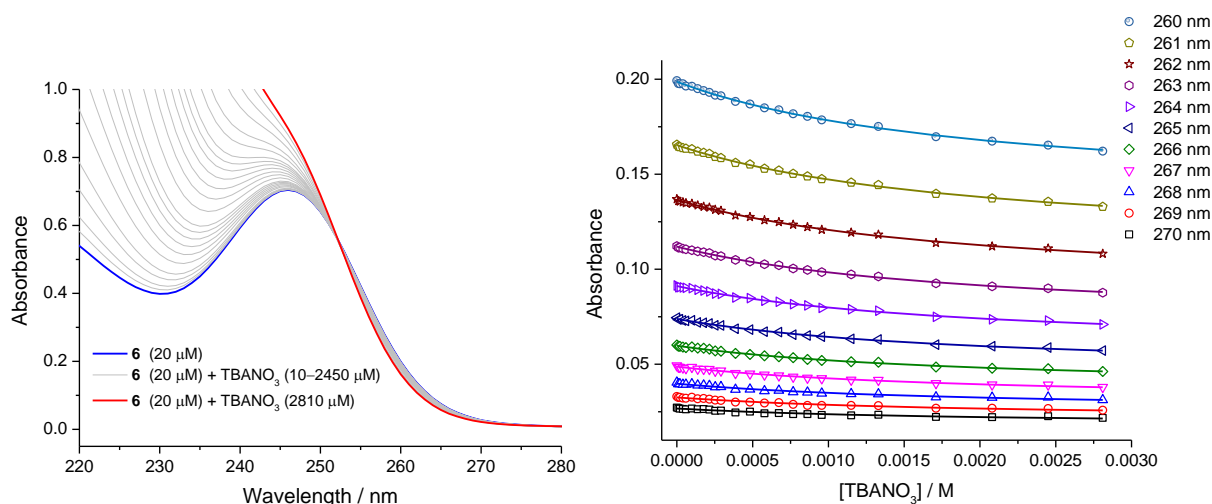


Fig. S21 UV-vis titration of **6** (20 μ M) with TBANO₃ (0–2.8 mM) in CH₃CN at 298 K. Global fitting of 11 absorbance values (260–270 nm) using the online BindFit software⁴ gave an association constant of 490 M⁻¹.

4. ISE chloride-nitrate exchange assay

4.1 General

ISE assays were conducted using POPC LUVs (mean diameter 200 nm) loaded with NaCl and suspended in NaNO₃. The LUVs were prepared as follows. A chloroform solution of POPC was evaporated in a round-bottom flask and the lipid film formed was dried under vacuum for at least 6 h. Then, the lipid film was hydrated by vortexing with an internal solution of NaCl (490 mM) buffered at pH 7.2 with 5 mM sodium phosphate salts. The lipid suspension was subjected to nine freeze/thaw cycles and then extruded 25 times through a 200 nm polycarbonate membrane. The vesicles were dialysed against an external solution of NaNO₃ (490 mM) buffered at pH 7.2 with 5 mM sodium phosphate salts for at least 2 h, and then diluted into a volumetric flask to obtain a vesicle stock suspension.

For each test, the vesicle stock suspension was diluted using the external solution to obtain a 5 mL sample containing 1 mM of lipid. A DMSO solution (25 µL) of the compound under study was added to the vesicle suspension to initiate anion transport, and the external chloride concentration was monitored by a chloride-selective electrode. At 5 min, a detergent (50 µL of 11% (w%) Triton X-100 in 7 : 1 (v/v) H₂O-DMSO) was added to lyse the vesicles and release all chloride to calibrate chloride efflux to 100%. The results were averaged over at least two repeats.

Hill plot analyses were performed with the test compound loaded at different concentrations. The chloride efflux at 270 s was plotted as a function of the compound concentration. Hill coefficients (n) and EC₅₀ (270 s) values were calculated by fitting the curves to the following equation:

$$y = y_0 + (y_{\max} - y_0) \frac{x^n}{K + x^n}$$

where y is chloride efflux (270 s) value with the compound loaded at concentration x , y_0 is the chloride efflux (270 s) value obtained without the compound, y_{\max} is the maximum chloride efflux (270 s) value, n is the Hill coefficient, and K is the EC₅₀ (270 s) value. The compound concentrations are expressed as compound-to-lipid molar ratios.

4.2 Kinetic data

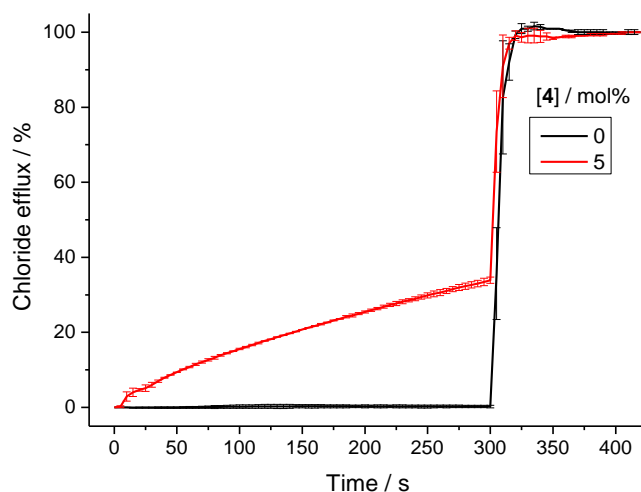


Fig. S22 Cl^- efflux facilitated by compound **4** measured in the ISE anion exchange assay. The vesicles were loaded with an internal solution of NaCl (490 mM) buffered at pH 7.2 with 5 mM sodium phosphate salts and suspended in an external solution of NaNO_3 (490 mM) buffered at pH 7.2 with 5 mM sodium phosphate salts. Compound **4** was added at 0 s, and detergent at 300 s. Compound concentrations are shown as compound-to-lipid molar ratios. Error bars represent standard deviations from at least two repeats.

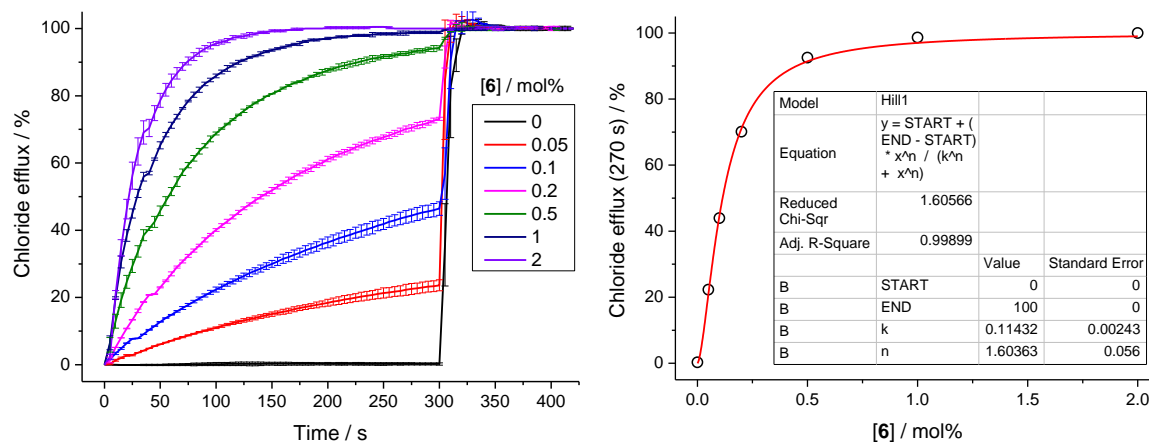


Fig. S23 Hill plot for $\text{Cl}^-/\text{NO}_3^-$ exchange facilitated by compound **6** measured in the ISE anion exchange assay. The vesicles were loaded with an internal solution of NaCl (490 mM) buffered at pH 7.2 with 5 mM sodium phosphate salts and suspended in an external solution of NaNO_3 (490 mM) buffered at pH 7.2 with 5 mM sodium phosphate salts. Compound **6** was added at 0 s, and detergent at 300 s. Compound concentrations are shown as compound-to-lipid molar ratios. Error bars represent standard deviations from at least two repeats.

5. HPTS assay

5.1 General

HPTS assays⁵ were conducted using POPC LUVs (mean diameter 200 nm) loaded with the pH-sensitive fluorescence dye HPTS (1 mM). The HPTS-loaded POPC LUVs were prepared as follows. A chloroform solution of POPC was evaporated in a round-bottom flask and the lipid film formed was dried under vacuum for at least 6 h. Then, the lipid film was hydrated by vortexing with an internal solution containing HPTS (1 mM) and NMDG-X (100 mM, X = Cl⁻ or NO₃⁻) buffered at pH 7.0 with 10 mM HEPES. The lipid suspension was subjected to nine freeze/thaw cycles and then extruded 25 times through a 200 nm polycarbonate membrane. The untrapped HPTS was removed by size exclusion chromatography on a Sephadex G-25 column using the external solution (with the same composition as the internal solution except that no HPTS was present), to obtain a vesicle stock suspension.

For each test, the vesicle stock suspension was diluted using the external solution to obtain a 2.2 mL sample containing 0.1 mM of lipid. The sample was stirred at 298 K and the fluorescence ratio of HPTS ($\lambda_{\text{ex}} = 460$ nm, $\lambda_{\text{em}} = 510$ nm divided by $\lambda_{\text{ex}} = 403$ nm, $\lambda_{\text{em}} = 510$ nm) was recorded over time.

A base pulse of NMDG (5 mM) was added to the vesicle sample to generate a pH gradient with inside pH 7 and outside pH 8. Subsequently, gramicidin D (if applicable, 0.1 mol%, added in 11 μ L of DMSO) and the compound under study (added in 11 μ L of DMSO) were added and the rate of the pH gradient dissipation was monitored by HPTS fluorescence. At the end of each measurement, a detergent (22 μ L of 11% (w%) Triton X-100 in 7 : 1 (v/v) H₂O-DMSO) was added to destroy the pH gradient to calibrate the assay. The fractional fluorescence intensity (I_f) was calculated using the following equation:

$$I_f = \frac{R_t - R_0}{R_f - R_0}$$

where R_t is the fluorescence ratio at time t , R_0 is the fluorescence ratio at time 0, and R_f is the final fluorescence ratio after detergent addition.

Hill plot analyses were performed with the test compound loaded at different concentrations. The fractional fluorescence intensity I_f at 200 s was plotted as a function of the compound concentration. Hill coefficients (n) and EC₅₀ (200 s) values were calculated by fitting the curves to the following equation:

$$y = y_0 + (y_{\text{max}} - y_0) \frac{x^n}{K + x^n}$$

where y is I_f (200 s) value with the compound loaded at concentration x , y_0 is the I_f (200 s) value obtained without the compound, y_{max} is the maximum I_f value, n is the Hill coefficient, and K is the EC₅₀ (200 s) value. The compound concentrations are expressed as compound-to-lipid molar ratios.

5.2 Hill plots for Cl⁻ transport

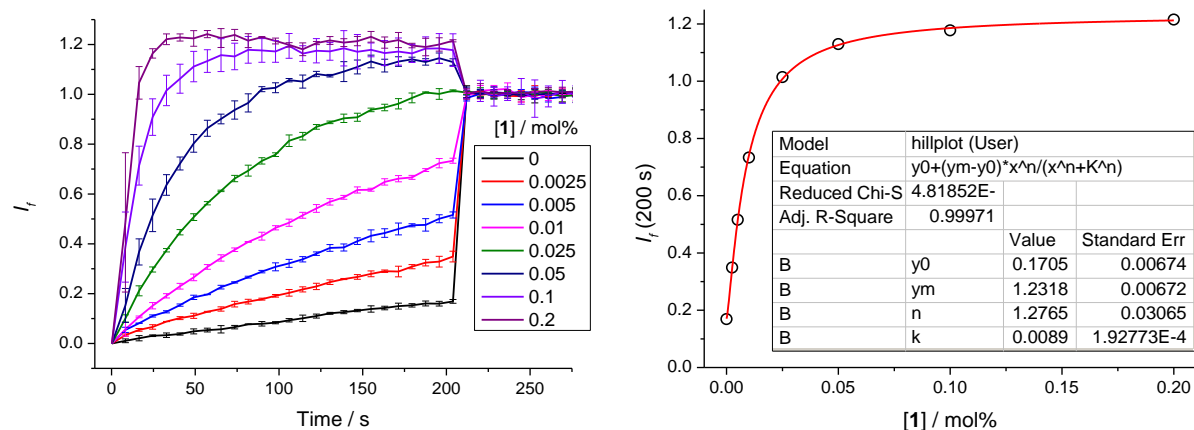


Fig. S24 Hill plot analysis of H⁺/Cl⁻ symport (or Cl⁻/OH⁻ antiport) facilitated by compound **1** measured in the HPTS assay. NMDG (5 mM) was added before the addition of **1** at 0 s, and detergent was added at 200 s. Compound concentrations are shown as compound-to-lipid molar ratios. Error bars represent standard deviations from at least two repeats.

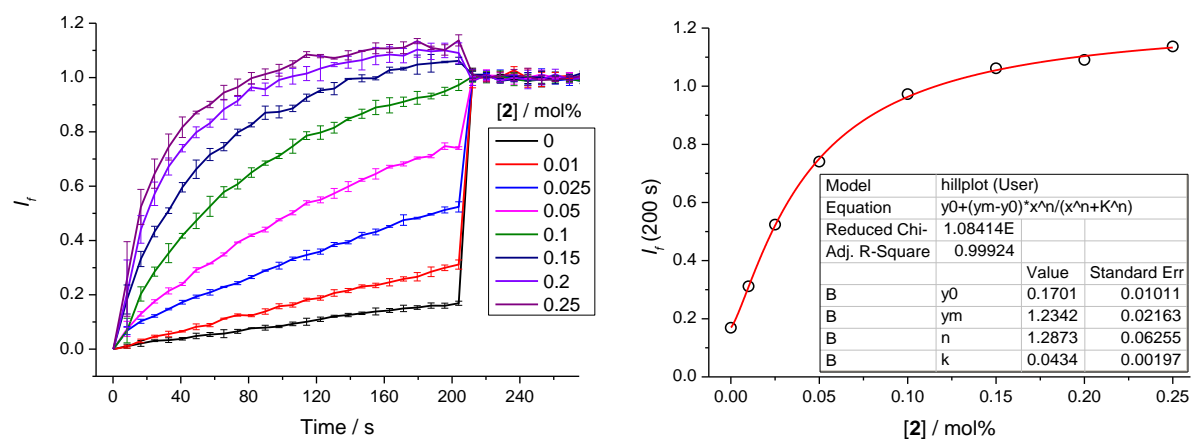


Fig. S25 Hill plot analysis of H⁺/Cl⁻ symport (or Cl⁻/OH⁻ antiport) facilitated by compound **2** measured in the HPTS assay. NMDG (5 mM) was added before the addition of **2** at 0 s, and detergent was added at 200 s. Compound concentrations are shown as compound-to-lipid molar ratios. Error bars represent standard deviations from at least two repeats.

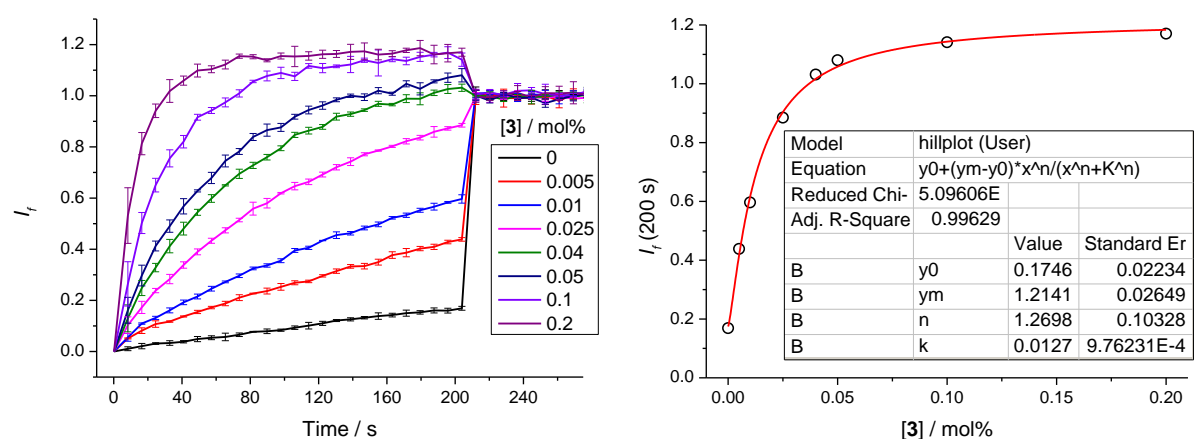


Fig. S26 Hill plot analysis of H⁺/Cl⁻ symport (or Cl⁻/OH⁻ antiport) facilitated by compound **3** measured in the HPTS assay. NMDG (5 mM) was added before the addition of **3** at 0 s, and detergent was added at 200 s. Compound concentrations are shown as compound-to-lipid molar ratios. Error bars represent standard deviations from at least two repeats.

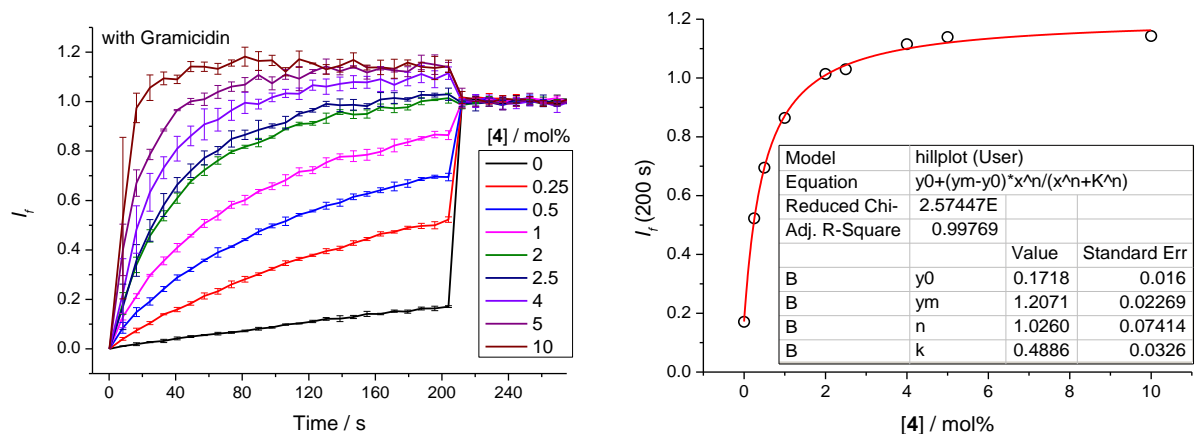


Fig. S27 Hill plot analysis of H^+/Cl^- symport (or Cl^-/OH^- antiport) facilitated by compound **4** measured in the HPTS assay. NMDG (5 mM) and gramicidin (0.1 mol%) were added before the addition of **4** at 0 s, and detergent was added at 200 s. Compound concentrations are shown as compound-to-lipid molar ratios. Error bars represent standard deviations from at least two repeats.

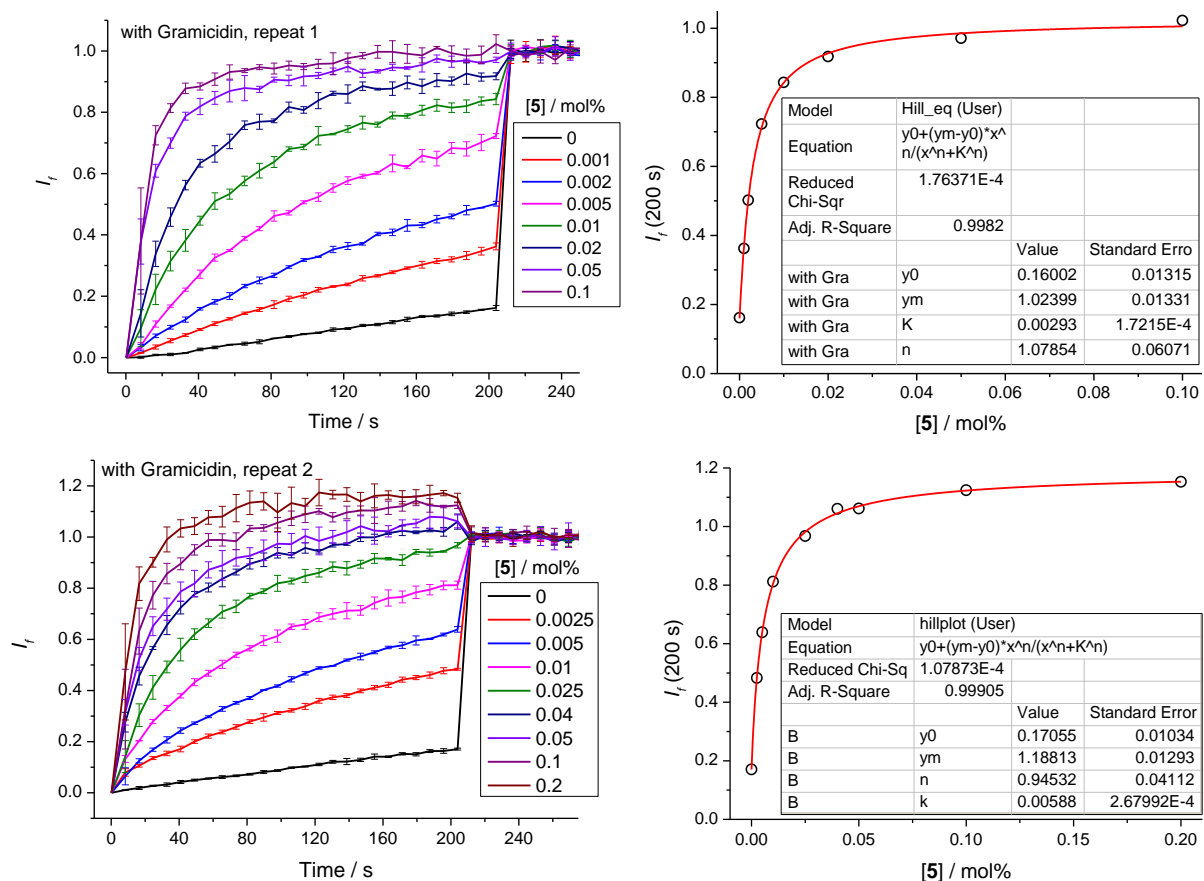


Fig. S28 Hill plot analysis of H^+/Cl^- symport (or Cl^-/OH^- antiport) facilitated by compound **5** measured in the HPTS assay. NMDG (5 mM) and gramicidin (0.1 mol%) were added before the addition of **5** at 0 s, and detergent was added at 200 s. Compound concentrations are shown as compound-to-lipid molar ratios. Error bars represent standard deviations from at least two repeats.

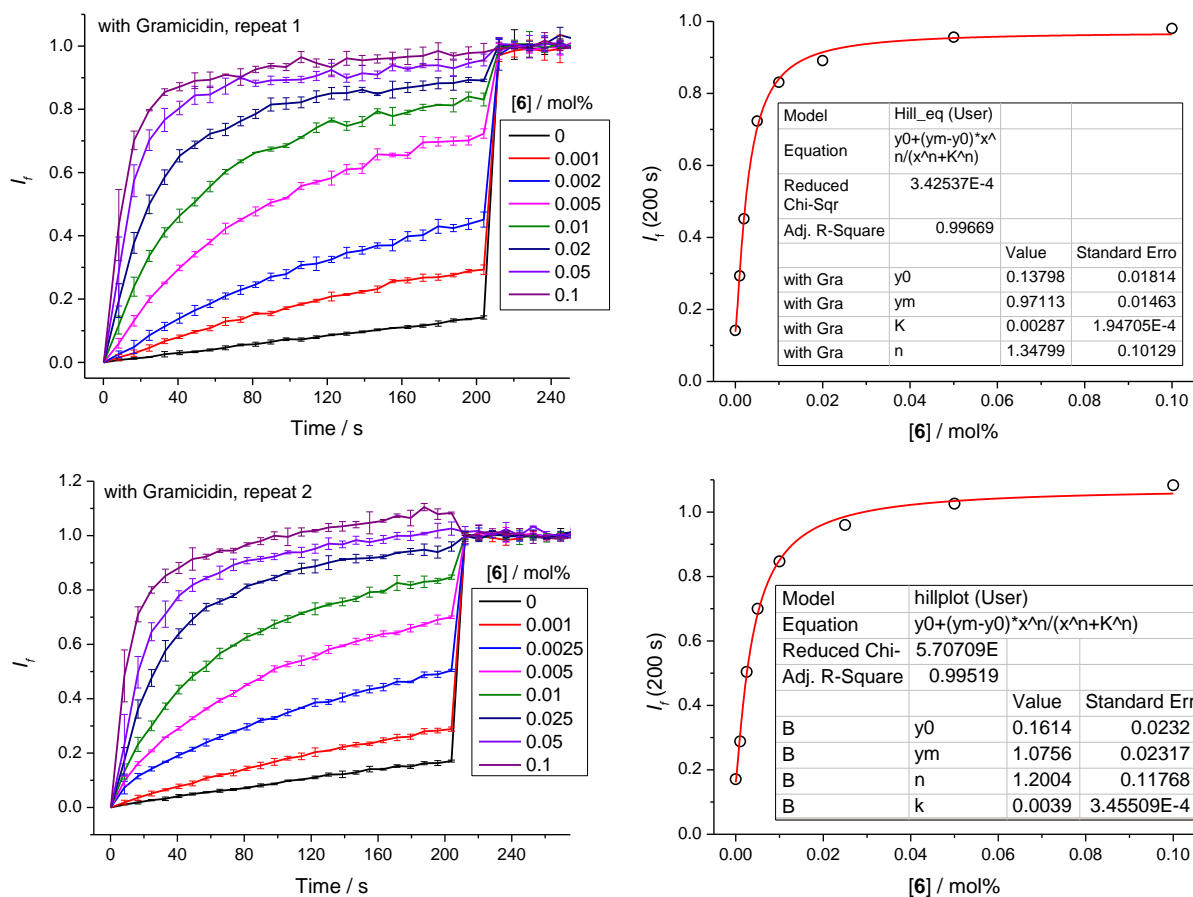


Fig. S29 Hill plot analysis of H^+/Cl^- symport (or Cl^-/OH^- antiport) facilitated by compound **6** measured in the HPTS assay. NMDG (5 mM) and gramicidin (0.1 mol%) were added before the addition of **6** at 0 s, and detergent was added at 200 s. Compound concentrations are shown as compound-to-lipid molar ratios. Error bars represent standard deviations from at least two repeats.

5.3 Hill plots for NO_3^- transport

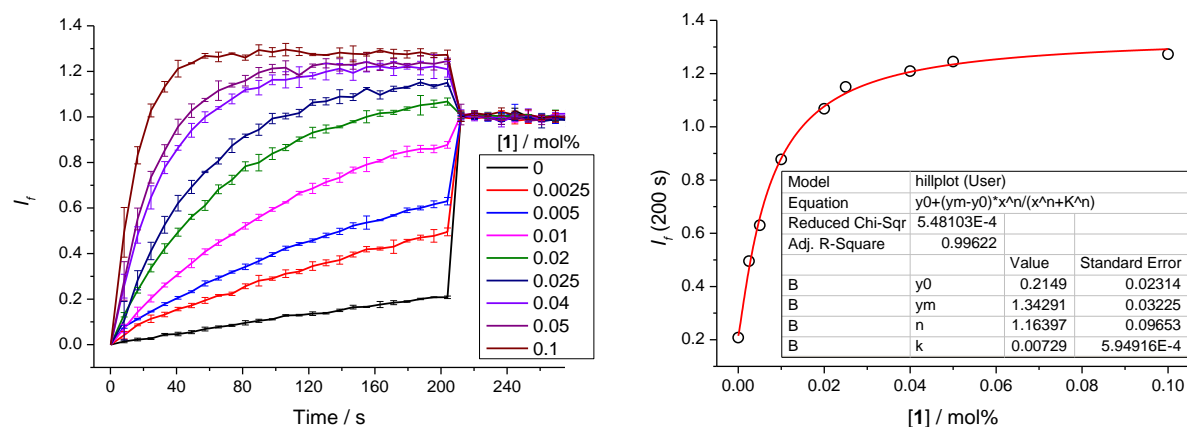


Fig. S30 Hill plot analysis of H^+/NO_3^- symport (or $\text{NO}_3^-/\text{OH}^-$ antiport) facilitated by compound **1** measured in the HPTS assay. NMDG (5 mM) was added before the addition of **1** at 0 s, and detergent was added at 200 s. Compound concentrations are shown as compound-to-lipid molar ratios. Error bars represent standard deviations from at least two repeats.

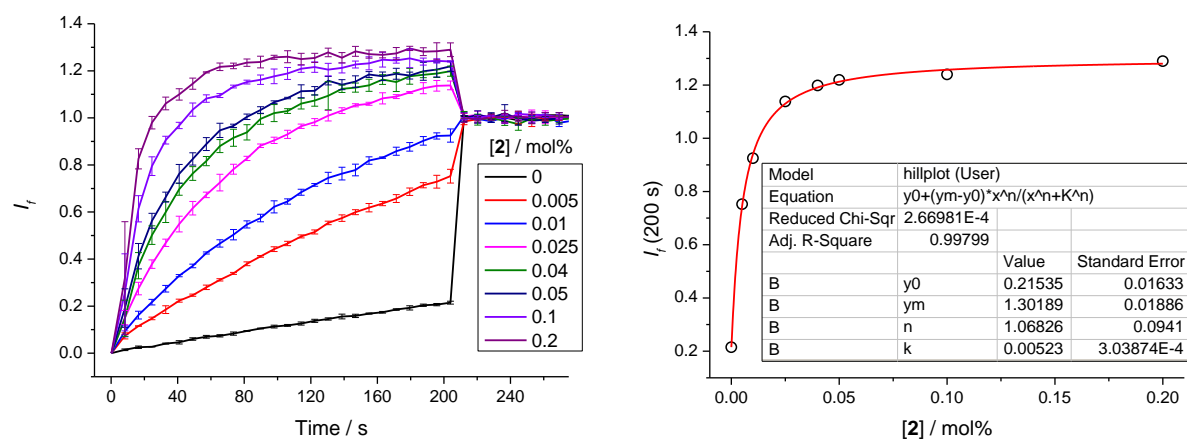


Fig. S31 Hill plot analysis of H^+/NO_3^- symport (or $\text{NO}_3^-/\text{OH}^-$ antiport) facilitated by compound **2** measured in the HPTS assay. NMDG (5 mM) was added before the addition of **2** at 0 s, and detergent was added at 200 s. Compound concentrations are shown as compound-to-lipid molar ratios. Error bars represent standard deviations from at least two repeats.

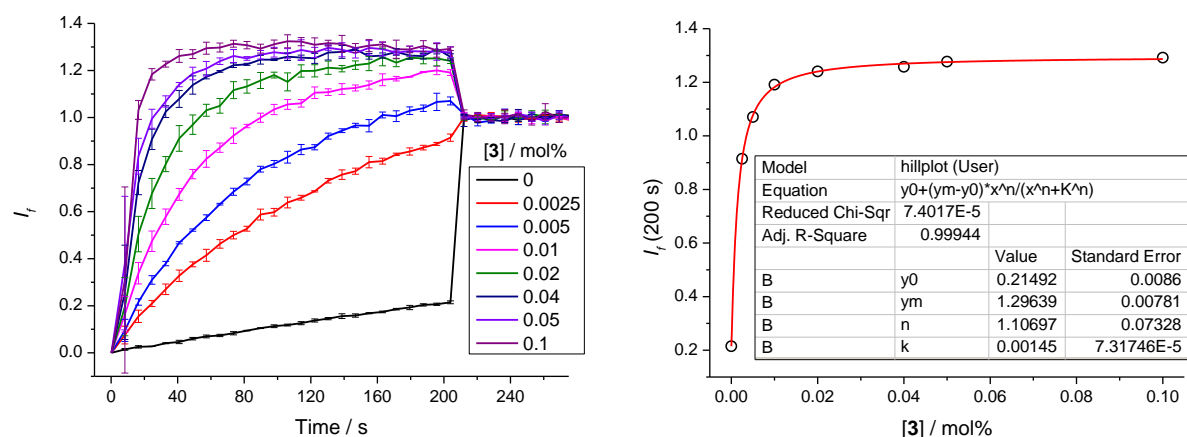


Fig. S32 Hill plot analysis of H^+/NO_3^- symport (or $\text{NO}_3^-/\text{OH}^-$ antiport) facilitated by compound **3** measured in the HPTS assay. NMDG (5 mM) was added before the addition of **3** at 0 s, and detergent was added at 200 s. Compound concentrations are shown as compound-to-lipid molar ratios. Error bars represent standard deviations from at least two repeats.

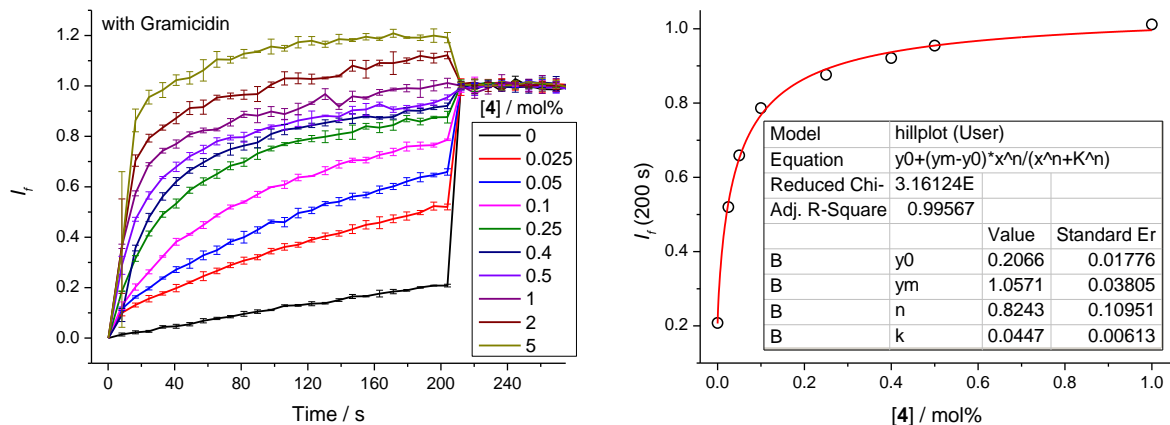


Fig. S33 Hill plot analysis of H^+/NO_3^- symport (or NO_3^-/OH^- antiport) facilitated by compound **4** measured in the HPTS assay. NMDG (5 mM) and gramicidin (0.1 mol%) were added before the addition of **4** at 0 s, and detergent was added at 200 s. Compound concentrations are shown as compound-to-lipid molar ratios. Error bars represent standard deviations from at least two repeats.

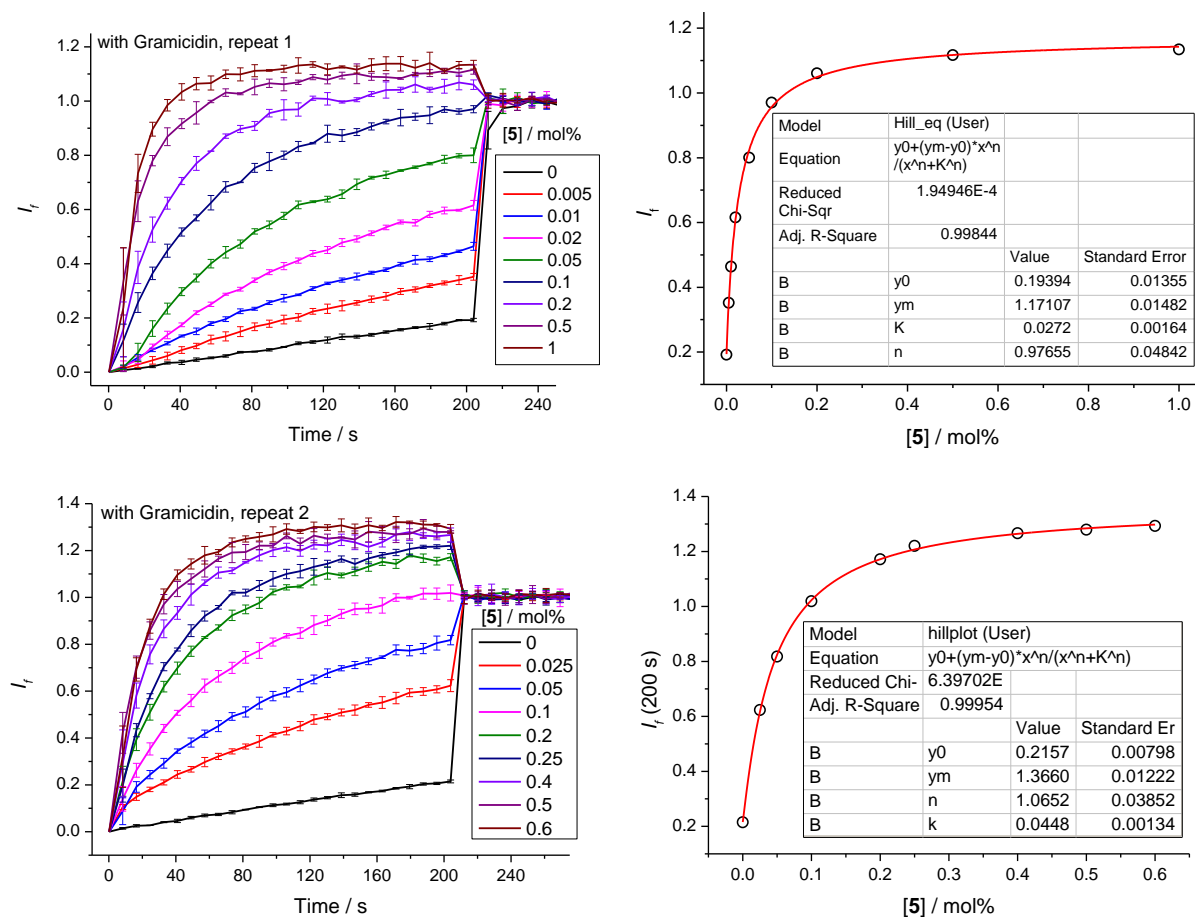


Fig. S34 Hill plot analysis of H^+/NO_3^- symport (or NO_3^-/OH^- antiport) facilitated by compound **5** measured in the HPTS assay. NMDG (5 mM) and gramicidin (0.1 mol%) were added before the addition of **5** at 0 s, and detergent was added at 200 s. Compound concentrations are shown as compound-to-lipid molar ratios. Error bars represent standard deviations from at least two repeats.

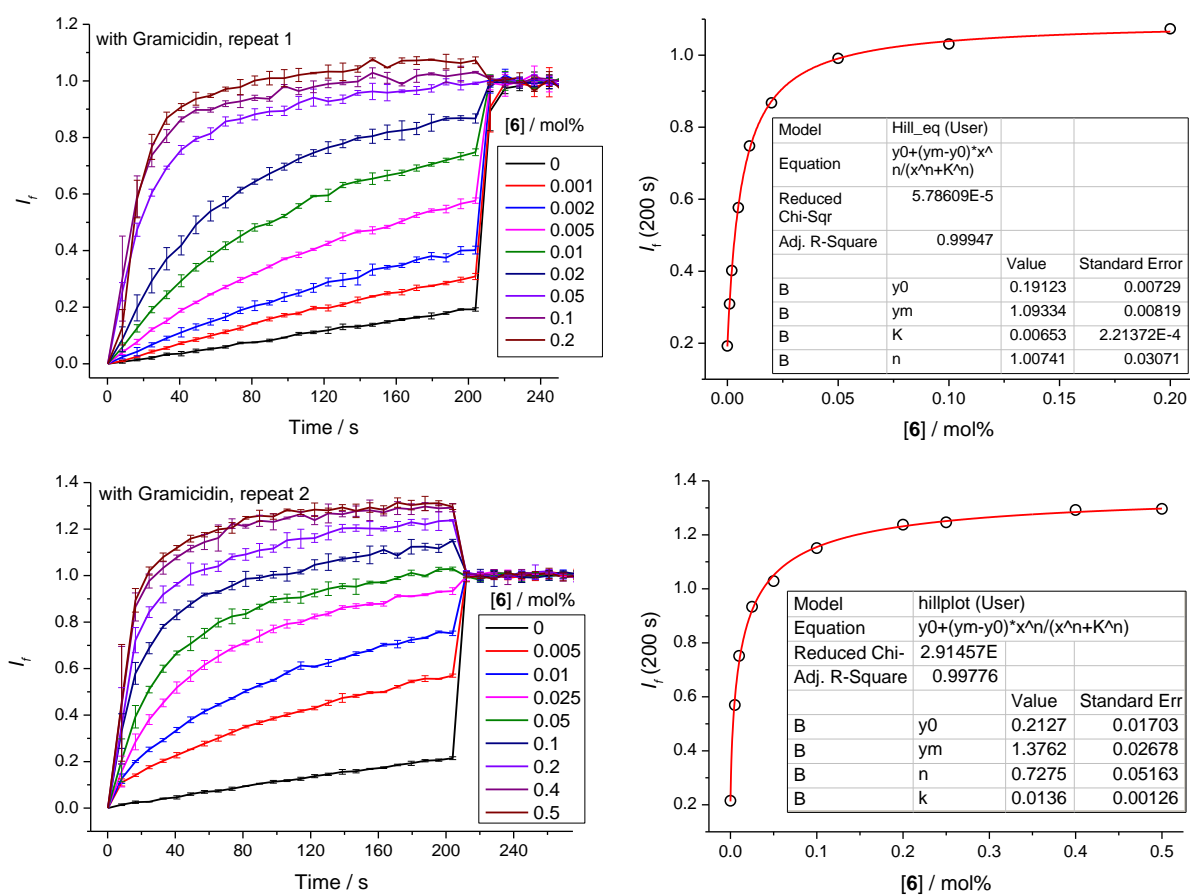


Fig. S35 Hill plot analysis of H^+/NO_3^- symport (or $\text{NO}_3^-/\text{OH}^-$ antiport) facilitated by compound **6** measured in the HPTS assay. NMDG (5 mM) and gramicidin (0.1 mol%) were added before the addition of **6** at 0 s, and detergent was added at 200 s. Compound concentrations are shown as compound-to-lipid molar ratios. Error bars represent standard deviations from at least two repeats.

6. Osmotic assay

6.1 General

The osmotic response assay was conducted using POPC LUVs (mean diameter 400 nm) prepared as follows. A chloroform solution of POPC was evaporated in a round-bottom flask and the lipid film formed was dried under vacuum for at least 6 h. Then, the lipid film was hydrated by vortexing with an internal solution of KX (300 mM, X = Cl⁻, Br⁻, or NO₃⁻) buffered at pH 7.4 with 5 mM HEPES, to obtain a vesicle suspension with a lipid concentration of 40 mM. The lipid suspension was subjected to nine freeze/thaw cycles, extruded 21 times through a 400 nm polycarbonate membrane and then diluted with the internal solution to a lipid concentration of 20 mM.

For each measurement, the vesicle stock suspension was diluted using the external solution (300 mM of potassium gluconate buffered at pH 7.4 with 5 mM HEPES), to obtain a 2.2 mL sample containing 0.2 mM of lipid. The sample was stirred at 298 K. Valinomycin (Vln) (added in 11 μL of DMSO), and the compound under study (added in 11 μL of DMSO) were added and the light scattering intensity was recorded over time using a fluorimeter ($\lambda_{\text{ex}} = 600 \text{ nm}$, $\lambda_{\text{em}} = 600 \text{ nm}$). KX efflux induced by a combination of valinomycin and an anion transporter led to vesicle dehydration, flattening and consequently an increase in light scattering intensity which is approximately linear to the amount of KX efflux.⁶

The intensity enhancement factor I/I_0 (where I is the light scattering intensity at time t , and I_0 is the light scattering intensity before compound addition) was plotted as a function of time. Hill plot analyses were performed with the test compound loaded at different concentrations. I/I_0 at 10 min was plotted as a function of the compound concentration. Hill coefficients (n) and EC_{50} (10 min) values were calculated by fitting the curves to the following equation:

$$y = y_0 + (y_{\text{max}} - y_0) \frac{x^n}{K + x^n}$$

where y is I/I_0 (10 min) value with the compound loaded at concentration x , y_0 is the I/I_0 (10 min) value obtained without the compound (with only valinomycin), y_{max} is the maximum I/I_0 (10 min) value, n is the Hill coefficient, and K is the EC_{50} (10 min) value. The compound concentrations are expressed as compound-to-lipid molar ratios.

In this assay, valinomycin by itself is found to induce slow KNO₃ efflux (but no efflux of more hydrophilic anions Cl⁻ and Br⁻) presumably because of formation of a valinomycin-K⁺-NO₃⁻ ion pair complex facilitating NO₃⁻ transport.

6.2 Hill plots for Cl⁻ transport

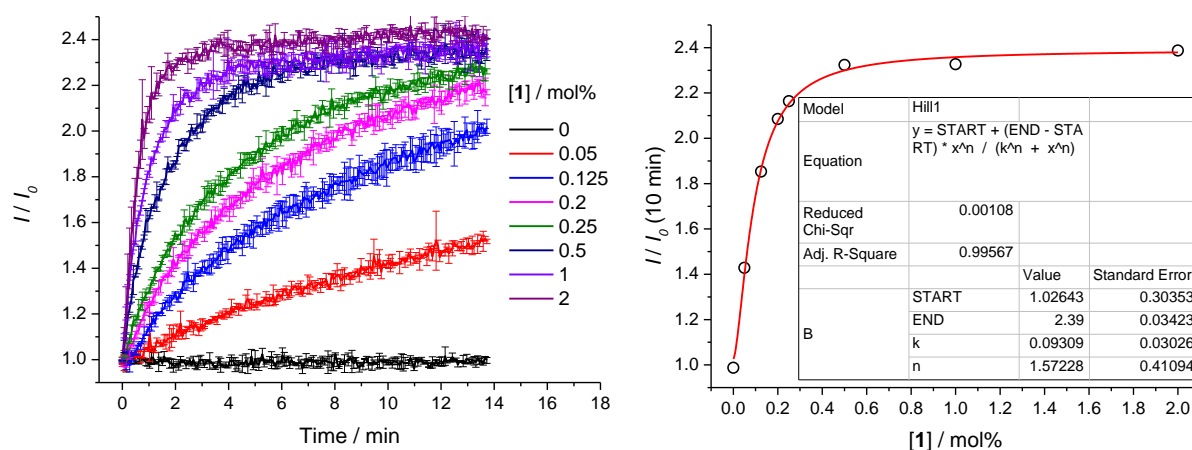


Fig. S36 Hill plot analysis of Cl⁻ transport facilitated by compound **1** measured in the osmotic assay. Vln (0.1 mol%) was added, before the addition of **1** at 0 s. Compound concentrations are shown as compound-to-lipid molar ratios. Error bars represent standard deviations from at least two repeats.

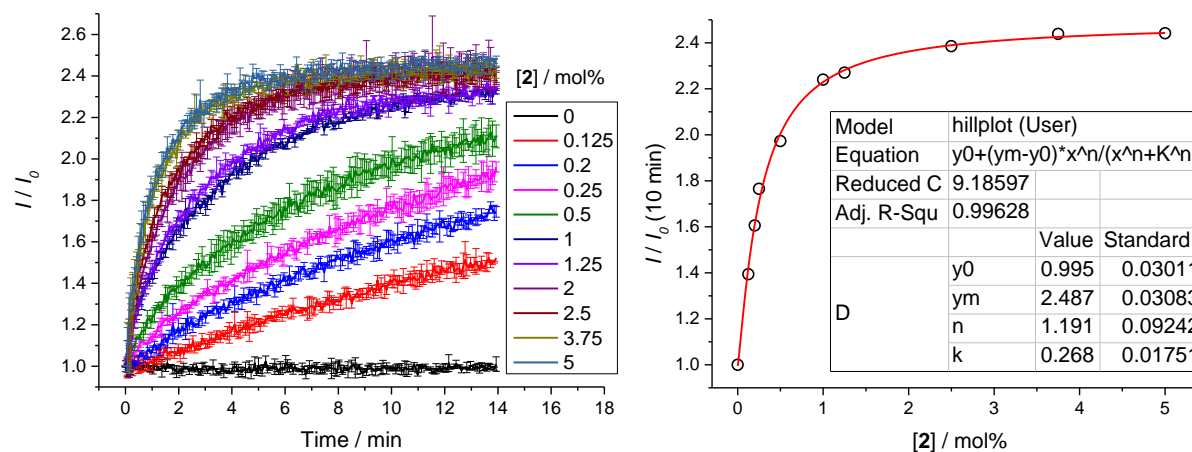


Fig. S37 Hill plot analysis of Cl⁻ transport facilitated by compound **2** measured in the osmotic assay. Vln (0.1 mol%) was added, before the addition of **2** at 0 s. Compound concentrations are shown as compound-to-lipid molar ratios. Error bars represent standard deviations from at least two repeats.

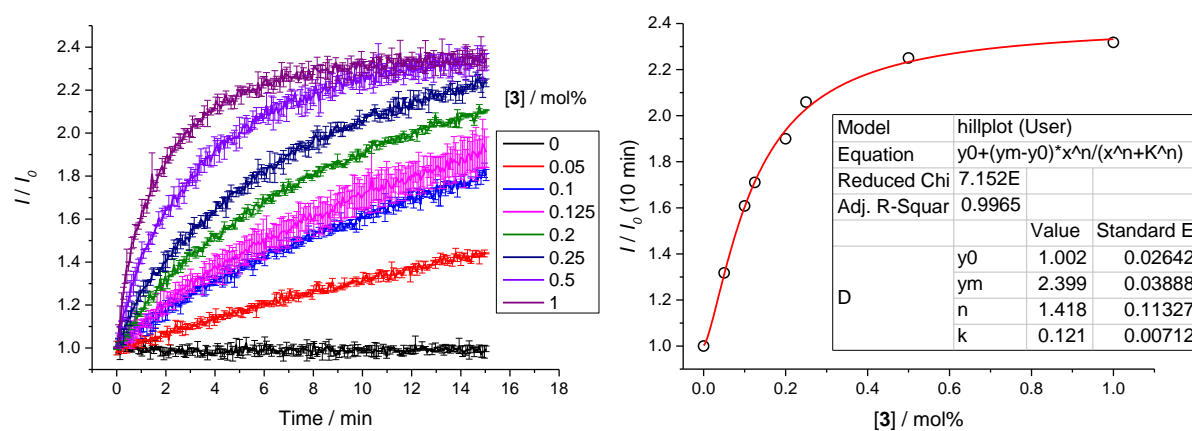


Fig. S38 Hill plot analysis of Cl⁻ transport facilitated by compound **3** measured in the osmotic assay. Vln (0.1 mol%) was added, before the addition of **3** at 0 s. Compound concentrations are shown as compound-to-lipid molar ratios. Error bars represent standard deviations from at least two repeats.

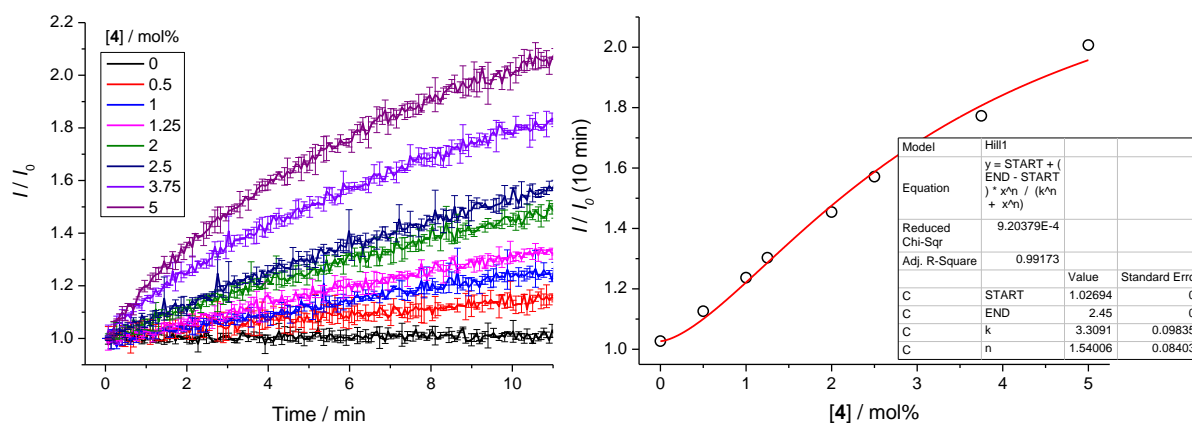


Fig. S39 Hill plot analysis of Cl^- transport facilitated by compound **4** measured in the osmotic assay. Vln (0.1 mol%) was added, before the addition of **4** at 0 s. Higher concentrations of **4** could not be used for Hill plots because of aggregation/precipitation of **4** affecting the light scattering intensity. In the Hill plot analysis, the end value was fixed at 2.45. This value had been determined by double exponential fitting of the kinetic curve of 5 mol% of **4**. Compound concentrations are shown as compound-to-lipid molar ratios. Error bars represent standard deviations from at least two repeats.

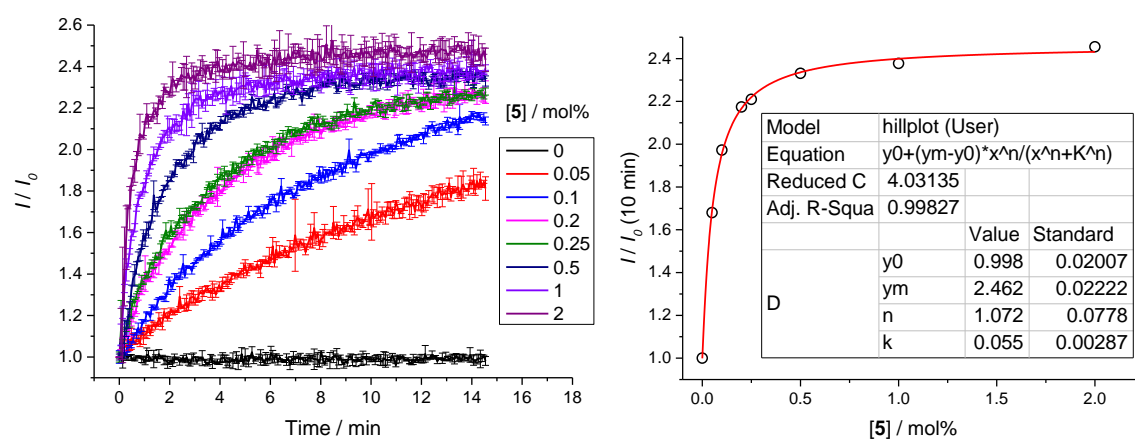


Fig. S40 Hill plot analysis of Cl^- transport facilitated by compound **5** measured in the Osmotic assay. Vln (0.1 mol%) was added, before the addition of **5** at 0 s. Compound concentrations are shown as compound-to-lipid molar ratios. Error bars represent standard deviations from at least two repeats.

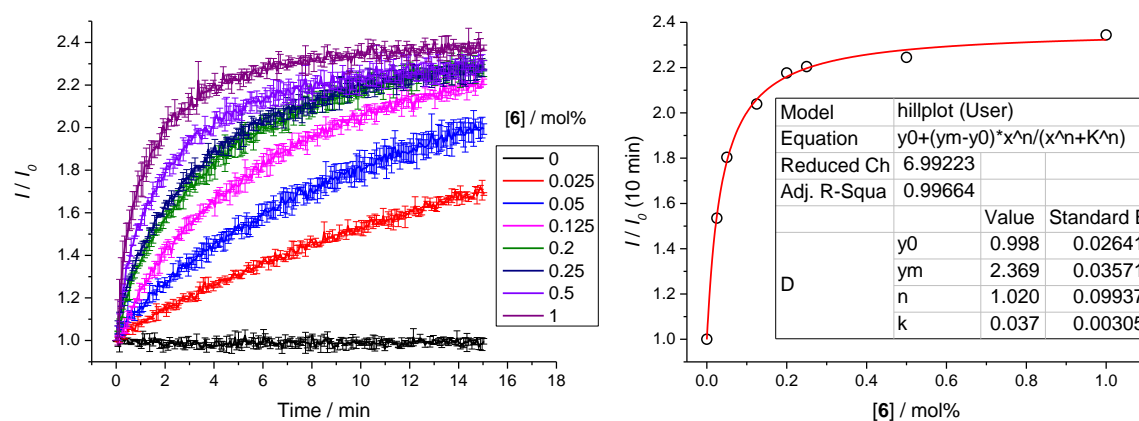


Fig. S41 Hill plot analysis of Cl^- transport facilitated by compound **6** measured in the Osmotic assay. Vln (0.1 mol%) was added, before the addition of **6** at 0 s. Compound concentrations are shown as compound-to-lipid molar ratios. Error bars represent standard deviations from at least two repeats.

6.3 Hill plots for NO_3^- transport

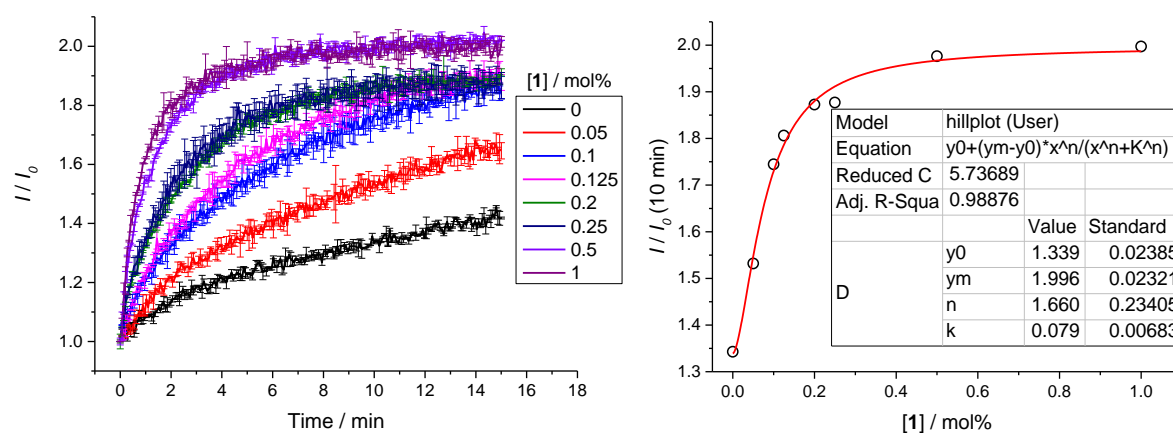


Fig. S42 Hill plot analysis of NO_3^- transport facilitated by compound **1** measured in the Osmotic assay. Vln (0.1 mol%) was added, before the addition of **1** at 0 s. Compound concentrations are shown as compound-to-lipid molar ratios. Error bars represent standard deviations from at least two repeats.

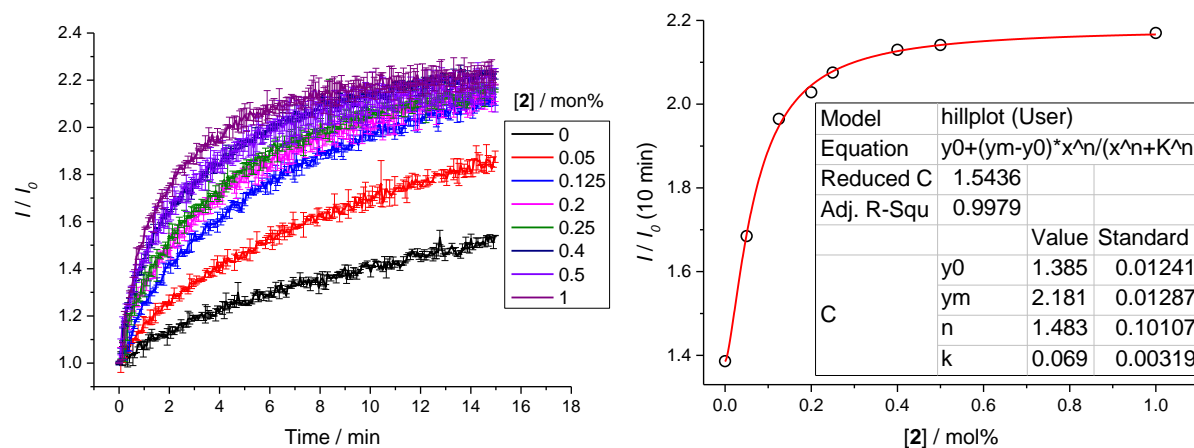


Fig. S43 Hill plot analysis of NO_3^- transport facilitated by compound **2** measured in the Osmotic assay. Vln (0.1 mol%) was added, before the addition of **2** at 0 s. Compound concentrations are shown as compound-to-lipid molar ratios. Error bars represent standard deviations from at least two repeats.

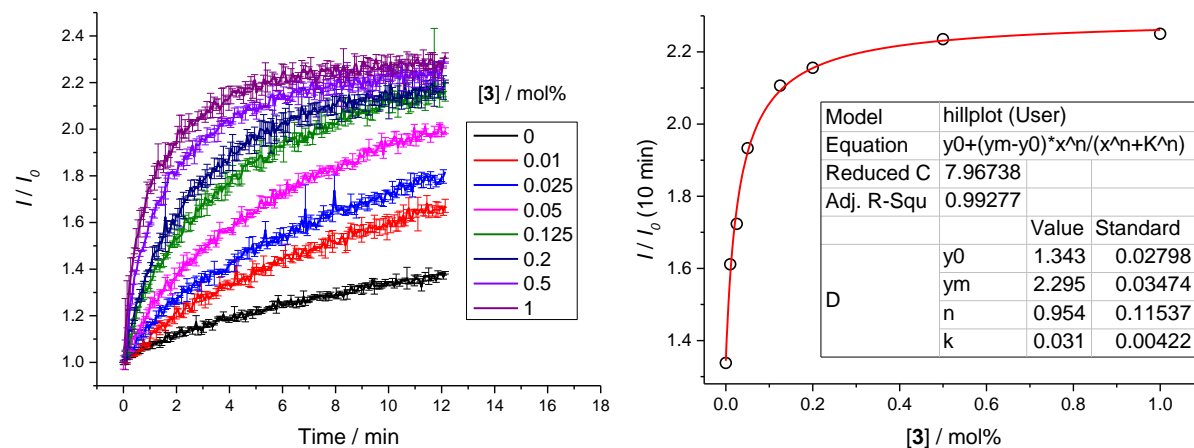


Fig. S44 Hill plot analysis of NO_3^- transport facilitated by compound **3** measured in the Osmotic assay. Vln (0.1 mol%) was added, before the addition of **3** at 0 s. Compound concentrations are shown as compound-to-lipid molar ratios. Error bars represent standard deviations from at least two repeats.

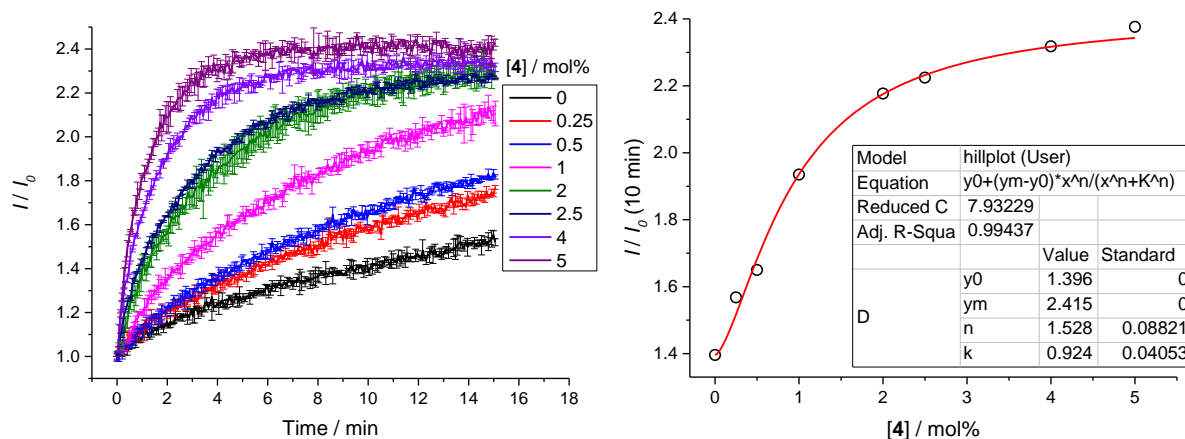


Fig. S45 Hill plot analysis of NO_3^- transport facilitated by compound **4** measured in the Osmotic assay. Vln (0.1 mol%) was added, before the addition of **4** at 0 s. Higher concentrations of **4** could not be used for Hill plots because of aggregation/precipitation of **4** affecting the light scattering intensity. In the Hill plot analysis, the end value was fixed at 2.42. This value had been determined by double exponential fitting of the kinetic curve of 5 mol% of **4**. Compound concentrations are shown as compound-to-lipid molar ratios. Error bars represent standard deviations from at least two repeats.

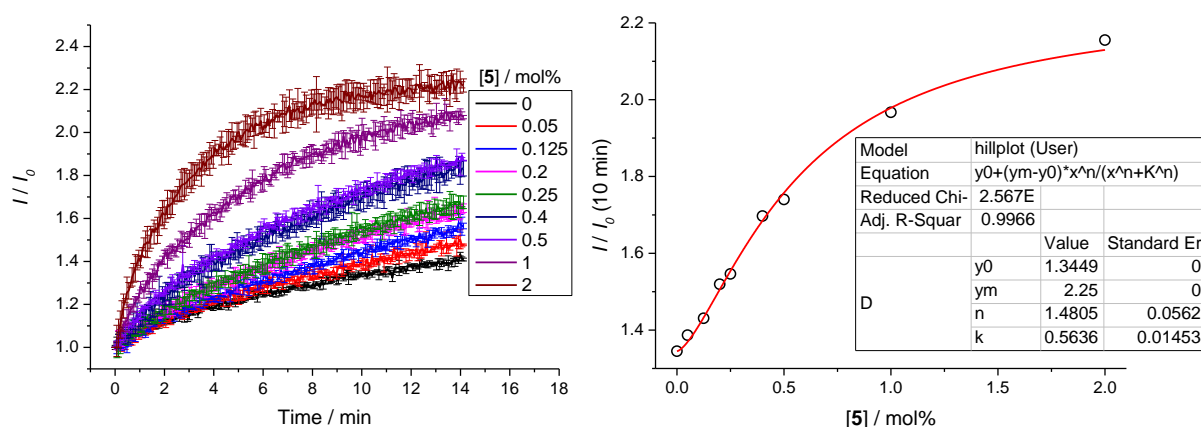


Fig. S46 Hill plot analysis of NO_3^- transport facilitated by compound **5** measured in the Osmotic assay. Vln (0.1 mol%) was added, before the addition of **5** at 0 s. Compound concentrations are shown as compound-to-lipid molar ratios. Error bars represent standard deviations from at least two repeats.

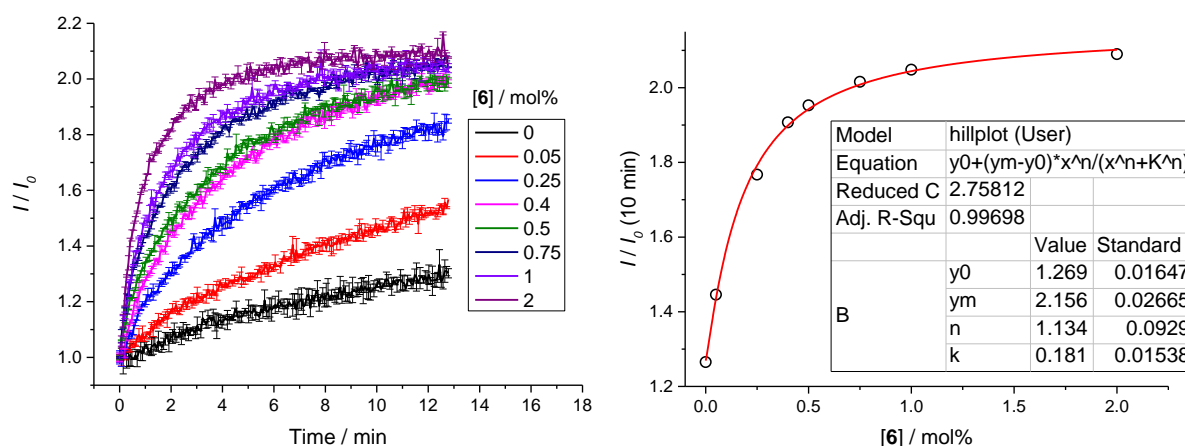


Fig. S47 Hill plot analysis of NO_3^- transport facilitated by compound **6** measured in the Osmotic assay. Vln (0.1 mol%) was added, before the addition of **6** at 0 s. Compound concentrations are shown as compound-to-lipid molar ratios. Error bars represent standard deviations from at least two repeats.

6.4 Br⁻ transport

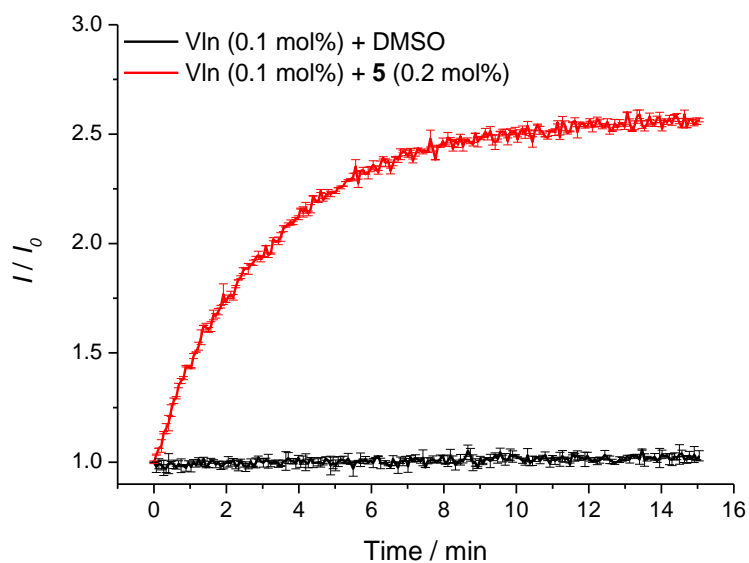


Fig. S48 KBr efflux facilitated by a combination of Vln and compound **5**. Vln (0.1 mol%) was added, before the addition of **5** at 0 s. Compound concentrations are shown as compound-to-lipid molar ratios. Error bars represent standard deviations from at least two repeats.

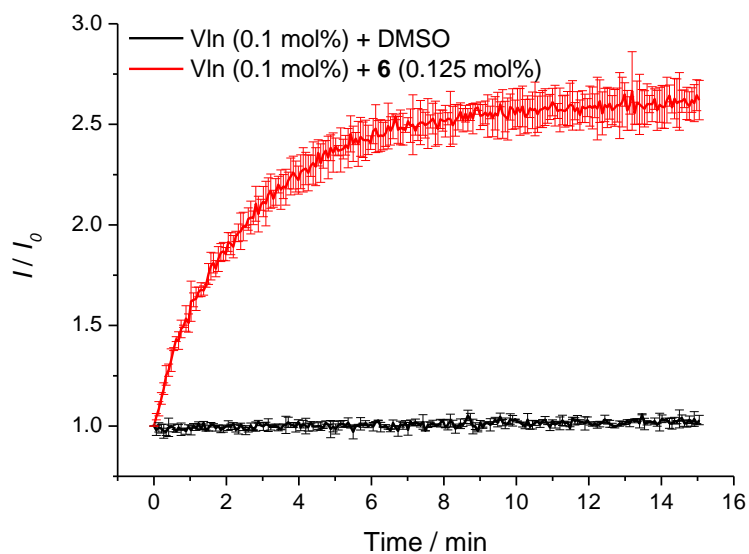


Fig. S49 KBr efflux facilitated by a combination of Vln and compound **6**. Vln (0.1 mol%) was added, before the addition of **6** at 0 s. Compound concentrations are shown as compound-to-lipid molar ratios. Error bars represent standard deviations from at least two repeats.

6.5 Single concentration comparison of anion transport

To compare the transport rate of different anions at a single transporter concentration, the half-life of the transport process was determined. The kinetic data were fitted to a two-phase exponential decay function in the OriginPro software:

$$y = y_0 + A_1 e^{-x/t_1} + A_2 e^{-x/t_2}$$

Then, the half-life $t_{1/2}$ was the x value corresponding to $y = y_0 + (A_1 + A_2)/2$. The transport rate was quantified using $1/t_{1/2}$. For nitrate transport, there is significant background transport of KNO_3 with valinomycin alone, and therefore the $t_{1/2}$ value of valinomycin alone was subtracted from the NO_3^- transport data.

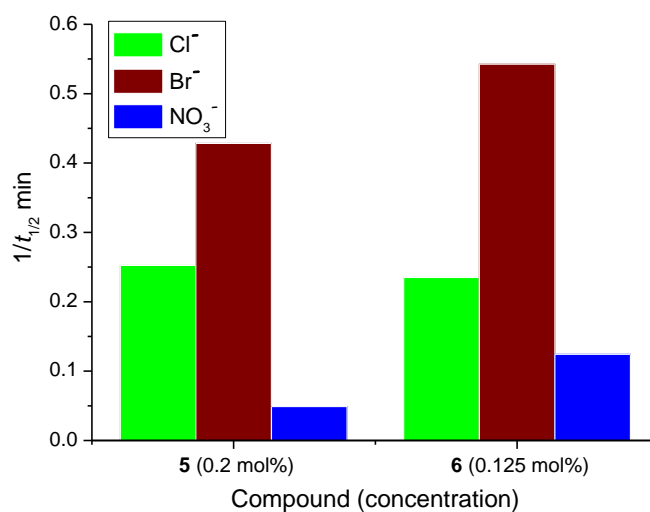


Fig. S50 Comparison of Cl^- , Br^- and NO_3^- transport facilitated by compounds **5** and **6** each at a single concentration, measured in the osmotic assay using Vln (0.1 mol%) to transport K^+ . Transport rates are shown as reciprocal of half-life ($1/t_{1/2}$). Compound concentrations are shown as compound-to-lipid molar ratios. In the case of NO_3^- transport, background transport of KNO_3 by Vln has been subtracted from the data.

7. Correlation between binding selectivity and transport selectivity

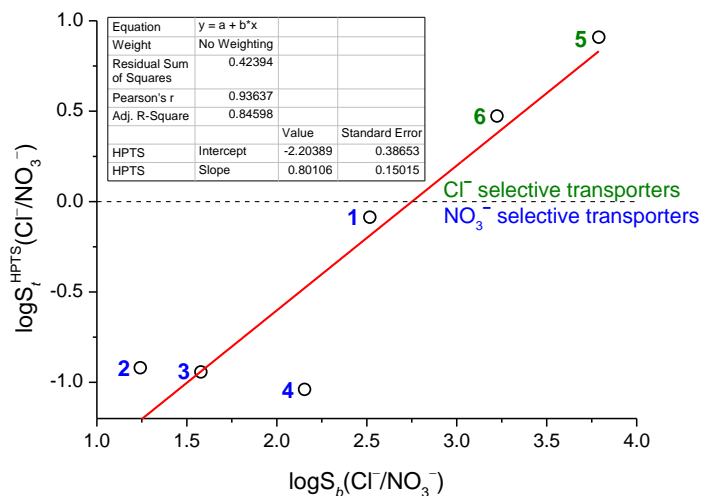


Fig. S51 Correlation between transport selectivity $\log S_t^{\text{HPTS}}(\text{Cl}^-/\text{NO}_3^-)$ and binding selectivity $\log S_b(\text{Cl}^-/\text{NO}_3^-)$. Compound numbers are shown next to the data points.

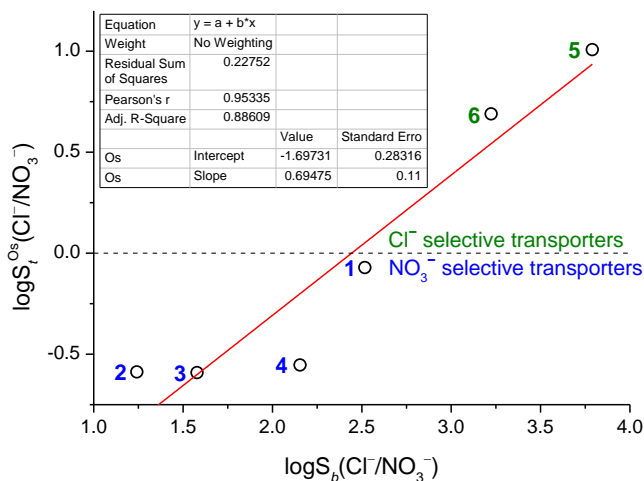


Fig. S52 Correlation between transport selectivity $\log S_t^{\text{Os}}(\text{Cl}^-/\text{NO}_3^-)$ and binding selectivity $\log S_b(\text{Cl}^-/\text{NO}_3^-)$. Compound numbers are shown next to the data points.

8. Normalised anion transport activities

The EC₅₀ values of compounds 1–6 determined under different assays were normalised to that of compound 1. The normalised activities were calculated using the following equation:

$$\text{Normalised activity (compound } \mathbf{x}) = \frac{1/\text{EC}_{50}(\text{compound } \mathbf{x})}{1/\text{EC}_{50}(\text{compound } \mathbf{1})}$$

Table S2 Normalised activities of compounds 1–6 under different assays

Compound	ISE exchange assay	HPTS assay (slower process)	Osmotic assay (slower process)
1	1.0	1.0	1.0
2	0.20	0.21	0.35
3	0.38	0.70	0.77
4	<0.01	0.018	0.030
5	0.19	0.25	0.17
6	0.55	0.88	0.51

9. Computational studies

The structures of the chloride and nitrate complexes of **5** were optimized with semi-empirical PM6 methods.⁷ The previously reported crystal structures of Cl⁻ and NO₃⁻ complexes of analogues of **5**⁸ were used as the starting conformations. PM6 optimizations were performed using the Gaussian 09 software package, revision B.01.⁹

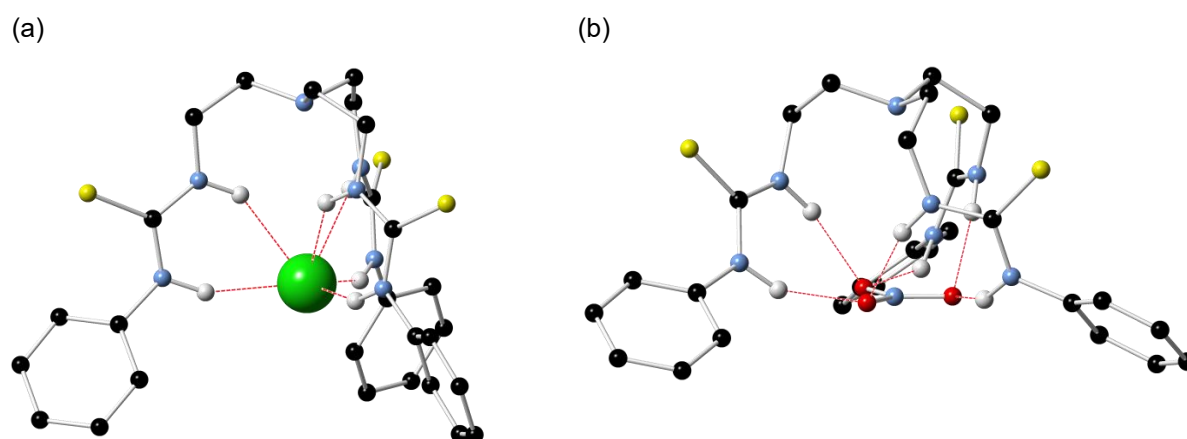


Fig. S53 PM6-optimised structures of Cl⁻ (a) and NO₃⁻ (b) complexes of **5** shown in ball-and-stick models. Most hydrogen atoms have been omitted for clarity. Hydrogen bonds are represented by red dashed lines.

10. References

- S1. N. Busschaert, I. L. Kirby, S. Young, S. J. Coles, P. N. Horton, M. E. Light and P. A. Gale, *Angew. Chem., Int. Ed.*, 2012, **51**, 4426-4430.
- S2. N. Busschaert, P. A. Gale, C. J. E. Haynes, M. E. Light, S. J. Moore, C. C. Tong, J. T. Davis and W. A. Harrell, Jr., *Chem. Commun.*, 2010, **46**, 6252-6254.
- S3. X. Wu, L. W. Judd, E. N. W. Howe, A. M. Withecombe, V. Soto-Cerrato, H. Li, N. Busschaert, H. Valkenier, R. Pérez-Tomás, D. N. Sheppard, Y.-B. Jiang, A. P. Davis and P. A. Gale, *Chem*, 2016, **1**, 127-146.
- S4. <http://supramolecular.org/> (accessed 19/06/2017).
- S5. S. Matile and N. Sakai, in *Analytical Methods in Supramolecular Chemistry*, ed. C. A. Schalley, Wiley-VCH, Weinheim, 2012, pp. 711-742.
- S6. R. B. Stockbridge, H.-H. Lim, R. Otten, C. Williams, T. Shane, Z. Weinberg and C. Miller, *Proc. Natl. Acad. Sci. USA*, 2012, **109**, 15289-15294.
- S7. J. P. Stewart, *J. Mol. Model.*, 2007, **13**, 1173-1213.
- S8. N. Busschaert, M. Wenzel, M. E. Light, P. Iglesias-Hernández, R. Pérez-Tomás and P. A. Gale, *J. Am. Chem. Soc.*, 2011, **133**, 14136-14148.
- S9. M. J. Frisch, G. W. Trucks, H. B. Schlegel, G. E. Scuseria, M. A. Robb, J. R. Cheeseman, G. Scalmani, V. Barone, B. Mennucci, G. A. Petersson, H. Nakatsuji, M. Caricato, X. Li, H. P. Hratchian, A. F. Izmaylov, J. Bloino, G. Zheng, J. L. Sonnenberg, M. Hada, M. Ehara, K. Toyota, R. Fukuda, J. Hasegawa, M. Ishida, T. Nakajima, Y. Honda, O. Kitao, H. Nakai, T. Vreven, J. A. Montgomery Jr., J. E. Peralta, F. Ogliaro, M. J. Bearpark, J. Heyd, E. N. Brothers, K. N. Kudin, V. N. Staroverov, R. Kobayashi, J. Normand, K. Raghavachari, A. P. Rendell, J. C. Burant, S. S. Iyengar, J. Tomasi, M. Cossi, N. Rega, N. J. Millam, M. Klene, J. E. Knox, J. B. Cross, V. Bakken, C. Adamo, J. Jaramillo, R. Gomperts, R. E. Stratmann, O. Yazyev, A. J. Austin, R. Cammi, C. Pomelli, J. W. Ochterski, R. L. Martin, K. Morokuma, V. G. Zakrzewski, G. A. Voth, P. Salvador, J. J. Dannenberg, S. Dapprich, A. D. Daniels, Ö. Farkas, J. B. Foresman, J. V. Ortiz, J. Cioslowski and D. J. Fox, Gaussian, Inc., Wallingford, CT, USA, 2009.